<u>CONSTRAINING KINEMATICS OF THE HELENA SALIENT, MONTANA</u>

A Thesis Presented to

the Faculty of the Department of Earth and Atmospheric Sciences

University of Houston

In Partial Fulfillment

of the Requirements for the Degree

Master of Science

By

Eileen Guthrie

December 2014

Constraining Kinematics of the Helena Salient, Montana

Eileen Guthrie

APPROVED:

Dr. Alexander Robinson, Advisor

Dr. Michael Murphy

Dr. Colin Shaw
Montana State University

Dean, College of Natural Sciences and Mathematics

ACKNOWLEDGEMENTS

I would like to thank Dr. Alex Robinson for his guidance and time. I would also like to thank Dr. Mike Murphy and Dr. Colin Shaw for direction and constructive feedback. Many thanks to the hosts of the Midland Valley Houston events for spending one-on-one time with me to develop my project and knowledge of the software. My deepest gratitude goes to my family and friends who supported me during the entire process.

CONSTRAINING KINEMATICS OF THE HELENA SALIENT, MONTANA

An Abstract of a Thesis

Presented to

the Faculty of the Department of Earth and Atmospheric Sciences

University of Houston

In Partial Fulfillment

of the Requirements for the Degree

Master of Science

By

Eileen Guthrie

December 2014

Abstract

The Helena Salient is a convex-to-the-foreland section of the Rocky Mountains in west-central Montana. It is comprised of Mesoproterozoic to Neoproterozoic sedimentary rocks overlain by a package of Paleozoic and Mesozoic sections. The salient contains three large east-directed thrust systems bounded by strike-slip zones to the north and south. This research explores the kinematic evolution of the Helena Salient and specific controls on the geometry of the salient.

Three forward models and cross sections were built to evaluate variations in shortening along the salient in order to investigate kinematic evolution. These models represent defining zones of salient development; the northern syntaxis, the central apex, and the southern portion. The northern cross section across the syntaxis has 25 km of shortening, the central cross section has 12 km of shortening, and the southern cross section has 14.5 km of shortening.

Restoration of all three cross sections was used to construct a finite displacement diagram for the Helena Salient and depict the initial position of the thrust faults within the salient. The measured magnitudes of displacement of the Helena Salient thrusts demonstrate that the initial position of the thrust faults coincides with deeper portions of the Belt Supergroup; suggesting pre-existing stratigraphic thicknesses were the primary control of initial formation of the Helena Salient. However, the larger shortening estimate from the northern syntaxis suggests a component of regional rotation of the cordilleran thrust belt may have exerted a significant control over the salient's kinematic evolution.

Contents

List of Abbreviations

DEM: Digital Elevation Model

HW: Hanging Wall

SWMTZ: Southwest Montana Transverse Zone

LET: Lombard Eldorado Thrust

LCL: Lewis and Clark Line

MMT: Moors Mountain Thrust

WCT: Willow Creek Thrust

VVT: Volcano Valley Thrust

1. Introduction

The Helena Salient is an arcuate section of the Rocky Mountain fold and thrust belt in central to southwestern Montana (Figure 1). Its geologic architecture is generally attributed to a complex history of Proterozoic continental breakup and Cordilleran orogenesis (Sears, 2007). The salient is composed of three major thrust systems that developed during the Late Cretaceous to early Cenozoic. The Campanian to Eocene thin-skinned contractional deformation and its 3-dimensional geometry is interpreted to be partially controlled by preexisting structures related to the middle Proterozoic Belt Basin, which is an east-west-trending allocogen thought to have a coincident southern margin with the Helena Salient (Price and Sears, 2000).

The Belt sedimentary rocks form an eastward-tapering Mesoproterozoic-Neoproterozoic sedimentary wedge that is topped by eastward tapering Paleozoic and Mesozoic sedimentary rocks (Winston, 1983). Thrusts in the region reflect this general eastward tapering trend and ramp upward from thick Belt Supergroup and younger strata in the west to thinner strata in the east. The differential thickness trend is illustrated by the palinspastic restoration of the Belt Supergroup in Figure 2, which depicts the thickness of the Belt Supergroup formation across the Helena salient (Price and Sears, 2000). This stratigraphic and structural framework is interpreted to control the formation of the Helena Salient and its current geometry.

General models of the kinematic evolution of salients describe different deformation patterns and assess salient formation using sandbox models and computer-generated models that provide insight into the kinematic evolution of salients (e.g.

Macedo and Marshak, 1999, Yonkee and Weil, 2010). The key components assessed in this study are along-strike shortening variations, and the development of a finite displacement model. The finite displacement model produced in this study indicates a kinematic evolution similar to the models produced by Yonkee and Weil, 2010, which compare a primary arc (a salient that begins as an arc and is translated into the foreland through uniform or radial slip) and a progressive arc (a salient that evolves into an arc through differential shortening and/or interlimb rotation) evolution. The primary arc uniform-slip models describe a situation similar to that of the Helena Salient as the model begins with an arc and through uniform slip is translated into the foreland which produces consistent shortening around the salient. This research presents an interpretation of the heterogeneous deformation pattern of the Helena Salient, uniform shortening in the southern portion of the Helena Salient, and increased shortening in the northern portion of the Helena Salient, and proposes an explanation of this pattern that differs from previously published models.

The goal of this research is to evaluate the kinematic evolution of the Helena Salient through compiling published geologic maps and building kinematic models to answer the following questions:

1. What is the restored geometry of the main thrust sheets within the Helena Salient?

2. What is a possible finite displacement pattern?

3. How does my restoration compare with analogue models?

4. Does the model support interpretations that the Helena Salient is a "basin-controlled" salient?

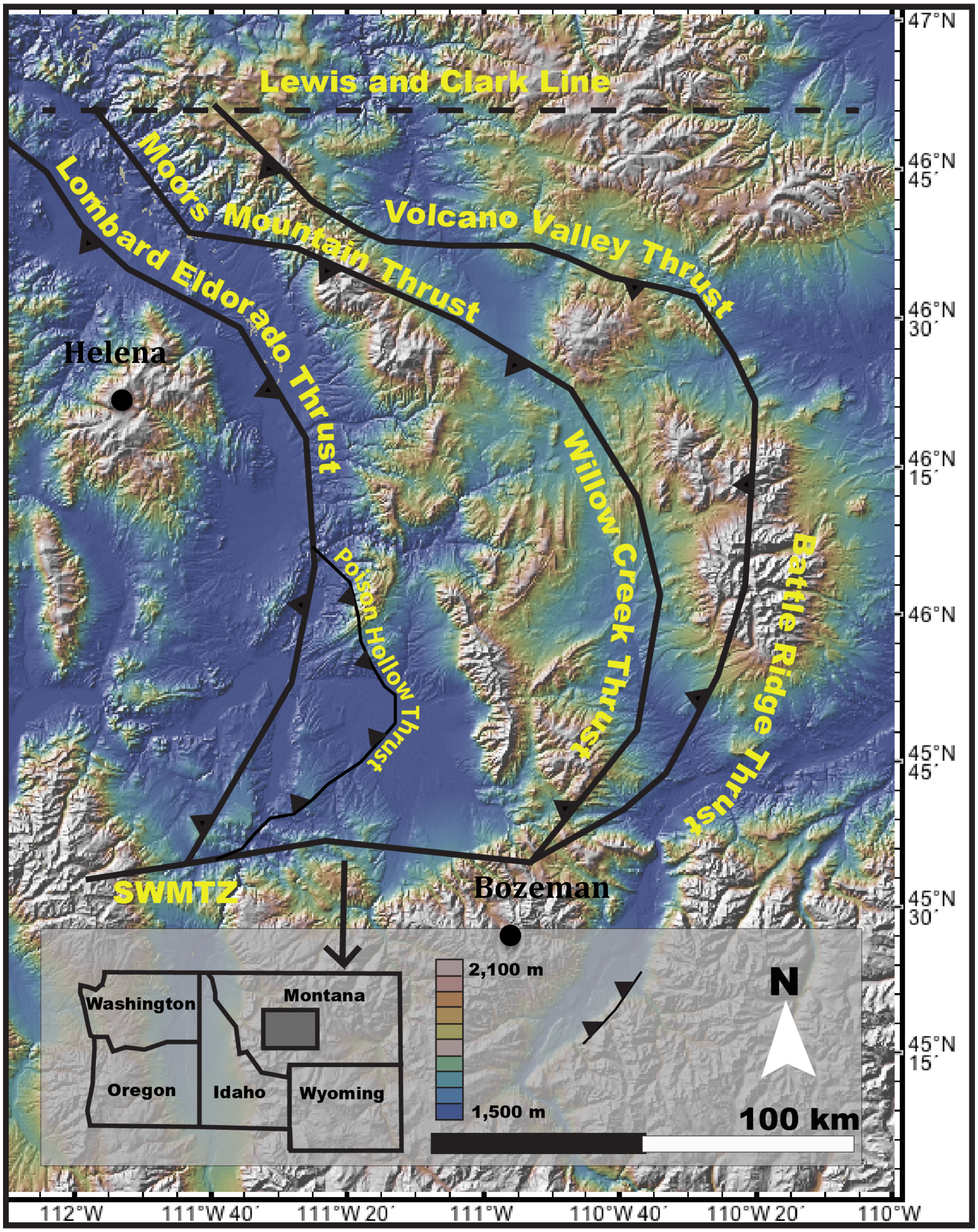

Figure 1: DEM of central Montana showing structures corresponding with the Helena Salient (DEM from Ryan et al., 2009).

2. Tectonic Framework

2.1 Proterozoic

The most important events of the Proterozoic relative to the formation of the Helena Salient are the tectonic genesis of the Belt Basin, the geometry of the structures bounding the basin, and the variations in thickness of the Belt Supergroup. Rifting during the Proterozic led to the development of an east-west-striking extensional system and the formation of a graben. This extensional system formed in a complex triple junction within the North American craton, which evolved into the Belt Basin (Figure 3) (Price and Sears, 2000).

The Belt Basin is bound by two transverse fault zones; the Southwest Montana Transverse Zone on the salient's southern margin, and the Lewis and Clark Line on its northern margin. The SWMTZ is interpreted to have formed during Proterozoic rifting as a rift bounding crustal scale normal fault. The LCL corresponds with a crustal-scale transpressional Cretaceous boundary feature that has been active intermittently since the Mesoproterozoic (Sears, 2006). These features have been interpreted as extensional fault systems associated with Proterozoic rifting (Sears, 2006).

The patterns of sedimentation (sandstone and shale that control flats and ramps) and thickness of the Belt Supergroup correspond to the graben into which the Belt Supergroup was deposited. The trough of the graben is over 5 km deep (based on sediment thickness estimates). The sediments range from 3-5 km thick around the study area with thickness decreasing from the core of the salient to the thrust front (Figure 2).

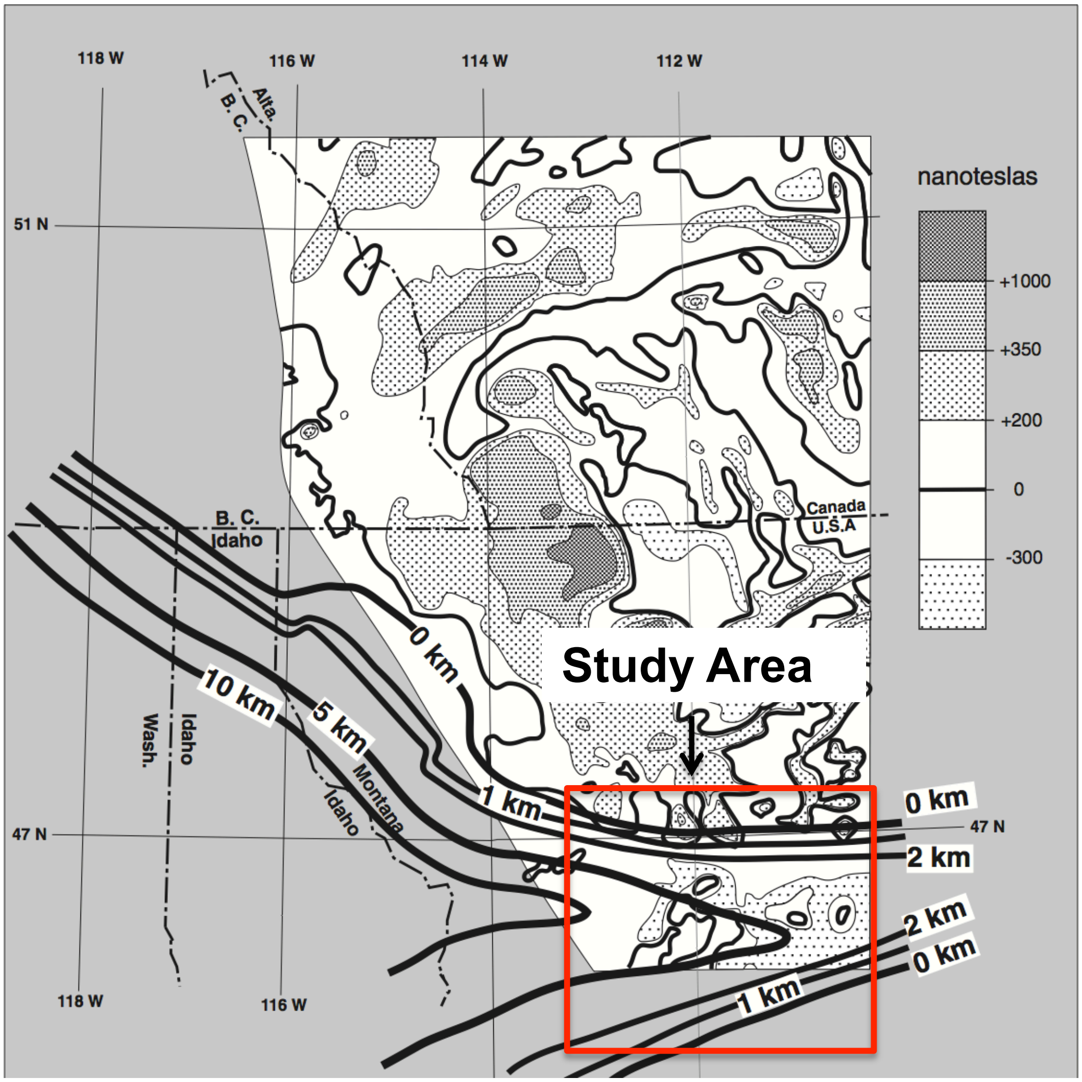

Figure 2: Palinspastic restoration of Lower Belt Supergroup thickness (Figure modified after Price and Sears, 2000).

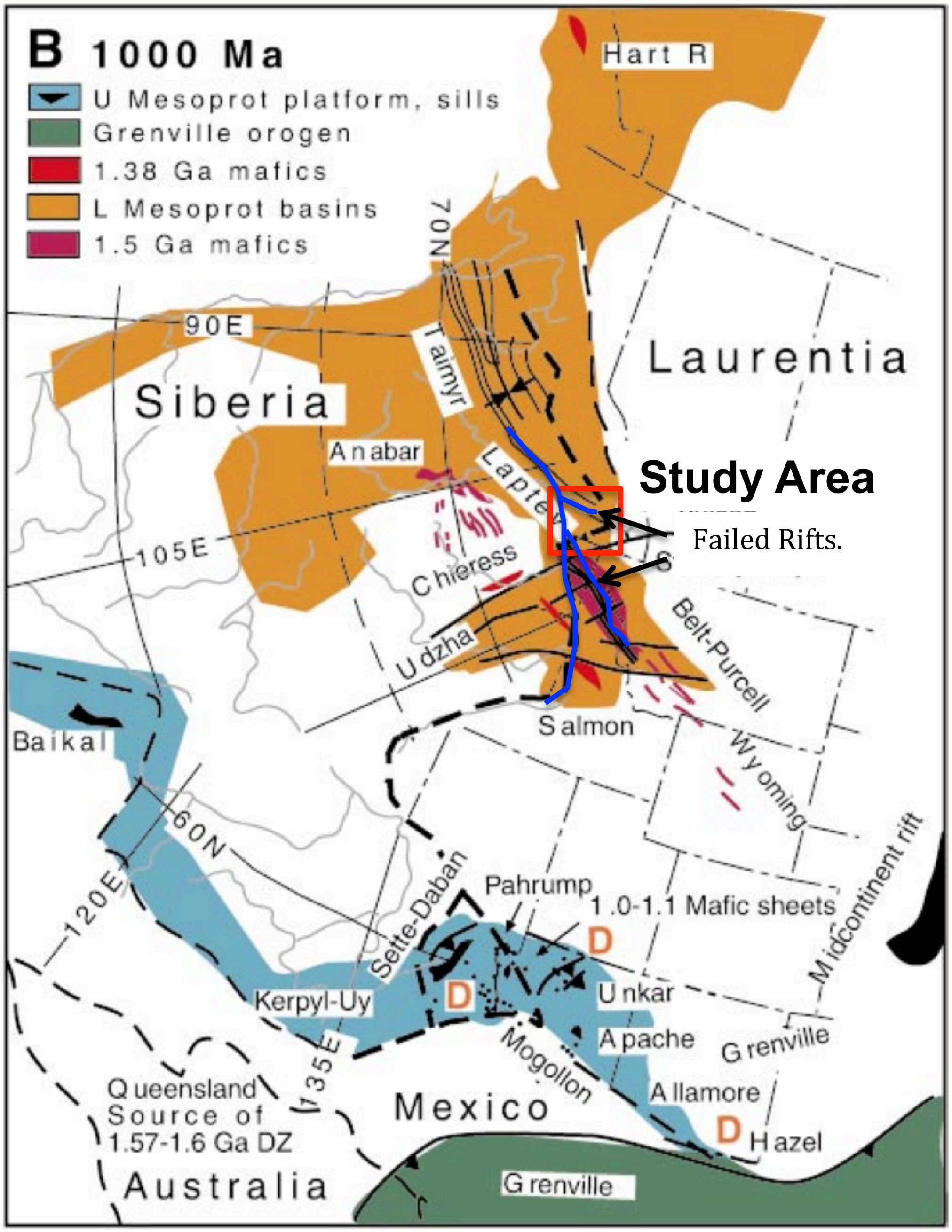

Figure 3: The Belt-Purcell basin is displayed in orange. This figure displays the formation of the Belt-Purcell basin as a consequence of a triple junction between Laurentia and Siberia where the basin formed as a failed rift. The rift system is displayed in blue. (Figure modified after Price and Sears, 2000).

2.2 Phanerozoic

The region was tectonically quiet and experienced various periods of marine and non-marine deposition until the middle Mesozoic. Then, subduction of the Farallon plate beneath the North American plate began in the Late Jurassic at a rate of 8 mm/yr and increased to 150 mm/yr in the Paleocene (DeCelles, 2004). As a result of the subducting Farallon plate, retroarc shortening of the Cordilleran thrust belt in western North America occurred around 155 Ma and lasted for the next 100 My (DeCelles, 2004). Deformation propagated eastward causing the initiation of the Lombard-Eldorado thrust as well as magmatic activity within the Helena Salient from 84-50 Ma. During formation of the salient, a decollement is interpreted to have formed at the base of the Belt Supergroup and propagated into the Phanerozoic rocks as thin skinned deformation and internal shortening migrated eastward (Winston, 1983).

The southern boundary of the salient is controlled by the SWMTZ, which marks the regional transition of thin-skin deformation in the north to thick-skin deformation in the south (Sears, 2006). It follows a Proterozoic crustal-scale structure discussed above and juxtaposes crystalline basement rocks of the Rocky Mountain foreland to the south against Phanerozoic sediments to the north. The SWMTZ reactivated around 75 Ma in the west coeval with formation of the Helena Salient and records 20- 50 km of displacement across its 720 km length with slip decreasing towards the foreland (Schmidt and O’Neill, 1982).

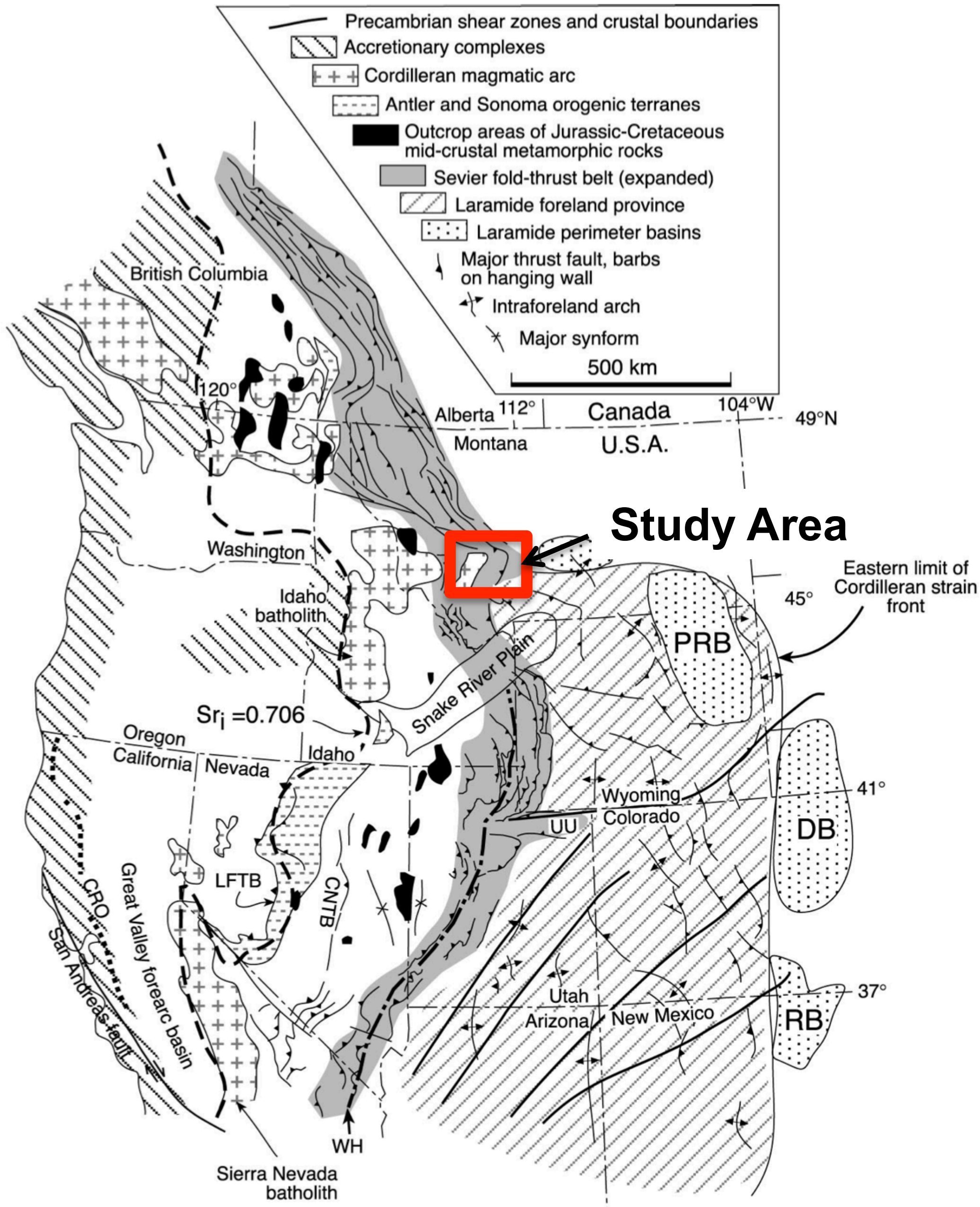

Figure 4: General tectonic map of Cretaceous western North America, showing the distribution of arc magmatism and deformation. (Figure modified after DeCelles, 2004).

2.3 Tectonostratigraphic Units

The base of the Helena Salient consists of thick Mesoproterozic- Neoproterozoic sedimentary units that are part of the Belt Supergroup. The Belt Supergroup unit is 2,000-5,000 m thick (Peterson, 1981) and consists of clastic, carbonate, and volcanic rocks that were deposited into an intracratonic rift, back-arc extensional, or strike-slip basin. The basin in which the Belt Supergroup sediments were deposited was bound to the south by the SWMTZ. This basin is interpreted to be an allocogen that formed during Proterozoic rifting of a continental margin of North America (Fryxell and Smith, 1983).

Following formation of the allocogen and deposition of the Belt Supergroup, a period of denudation that marks the boundary between the Proterozoic and Cambrian units, the next major stratigraphic sequence are Paleozoic units, primarily thick carbonates with lesser amounts of sandstones and shales that are cumulatively about 1,800 m thick (Woodward, 1981). The first Paleozoic group which unconformably overlies the Belt Supergroup is the Cambrian Flathead Sandstone, which is overlain, in turn, by thin cycles of Cambrian shales and carbonates. Ordovician rocks are of minor importance in this study due to poor exposures and possible absence throughout the study area. The relatively thin Cambrian succesion is overlain by the Middle Paleozoic Devonian units. The Devonian units are the Maywood, Jefferson, Three Forks, and Sappington Formations. These are mostly carbonate capped by shale and sandstone that were deposited in a shallow marine environment. Above the Devonian units are the lithologically strong Mississippian strata, consisting of the Madison Group and the Big Snowy Group. Finally, the lithologically weakest group of the preorogenic rocks are the

>610 m thick Mesozoic shales and sandstones, including the Morrison and Kootenai Formations, Colorado Group, and Blackleaf Formation. These units are composed of pre-Cretaceous shallow marine clastics and Cretaceous continental to nearshore marine facies. Synorogenic deposition begin in the late Cretaceous with the Two Medicine Formation and the Livingston Group (Peterson, 1981). The forward models described in the following section utilize only the pre-orogenic sequences (Figure 5).

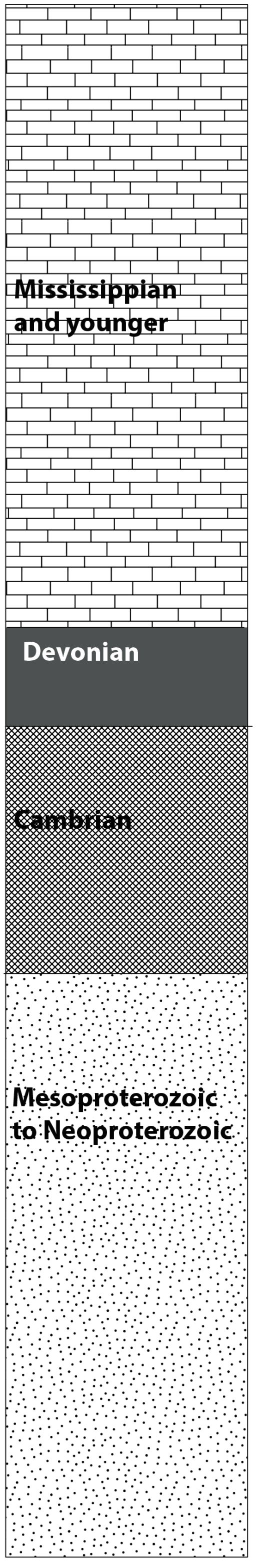

Cretaceous Morrison formation, Kootenai formation, Colorado group, and Blackleaf formation- Mississippian group; Lodgepole limestone and Mission Canyon limestone. Modeled thickness: 1.2 km

Devonian units include the Maywood, Jefferson, Three Forks, and Sappington Formations, mostly carbonate with a shale and sandstone cap. Modeled thickness: .24 km

Cambrian Flathead sandstone, Wolsey shale, Meagher limestone, and Park shale. Modeled thickness: .39 km

Mesoproterozic- Neoproterozoic sedimentary units of the Belt Supergroup. Modeled thickness: 5 km

Figure 5: Tectonostratigraphic column. (McDonald et al., 2005, Reynolds and Brandt, 2006, Berg et al., 2000, Vuke et al., 2014)

3. Geology of the Helena Salient

3.1 Thrusts of the Helena Salient

The Helena Salient is ~120 km long (E-W direction) and ~120 km wide (N-S direction), and is composed of three major thrust sheets that are interpreted to have initiated from west to east (Figure 6). In the west, the west-dipping Lombard-Eldorado is the oldest thrust, and brought Proterozoic Belt Supergroup rocks over Paleozoic and Mesozoic strata beginning in the Campanian. The next major thrusts to the east of the Lombard-Eldorado are the Willow Creek and Moors Mountain thrust system. To the east of the Willow Creek and Moors Mountain thrusts is the Volcano Valley thrust that links with the Battle Ridge thrust in the south. The Willow Creek fault system and the Volcano Valley faults are steeply dipping with en echelon folds in the hanging wall that imply left-lateral slip and reverse motion. These faults sole into a single thrust above crystalline basement rock at the base of the Belt Supergroup (Schmidt and O'Neill, 1982). Minimum shortening estimates across the Helena Salient yield 125 km, with a shortening rate of 8.3 mm/yr from middle Campanian to Late Paleocene (Fuentes et al., 2012).

In regards to internal deformation of the Helena Salient, Harlan et al. (2008) documents no vertical-axis rotation in the Lombard- Eldorado thrust sheet along its southern margin, which lies along the SWMTZ. Conversely, a similar study by Eldredge and Van der Voo (1988) documented as much as 54 degrees of clockwise rotation as a result of right-lateral sip along the SWMTZ on the southern border of the Helena Salient. Jolly and Sheriff (1992) also show a 39 degree clockwise rotation at the northern border of the Helena Salient. Regionally, Sears (2007) postulates regional vertical axis rotation in this area around a clockwise pole that effects the Lombard- Eldorado thrust sheet due to possible Farralon plate rotation beneath the North American craton as shown in Figure 7 (Sears, 2006). Sears used restored basement involved ranges and restored Belt thrust slabs to calculate the amount of rotation necessary to produce current day thrust geometry. In the insert in Figure 7, B represents the initial position corresponding to pole B and B' represents the final position after rotation around pole B occurred, this is the same with pole A, A, and A'.

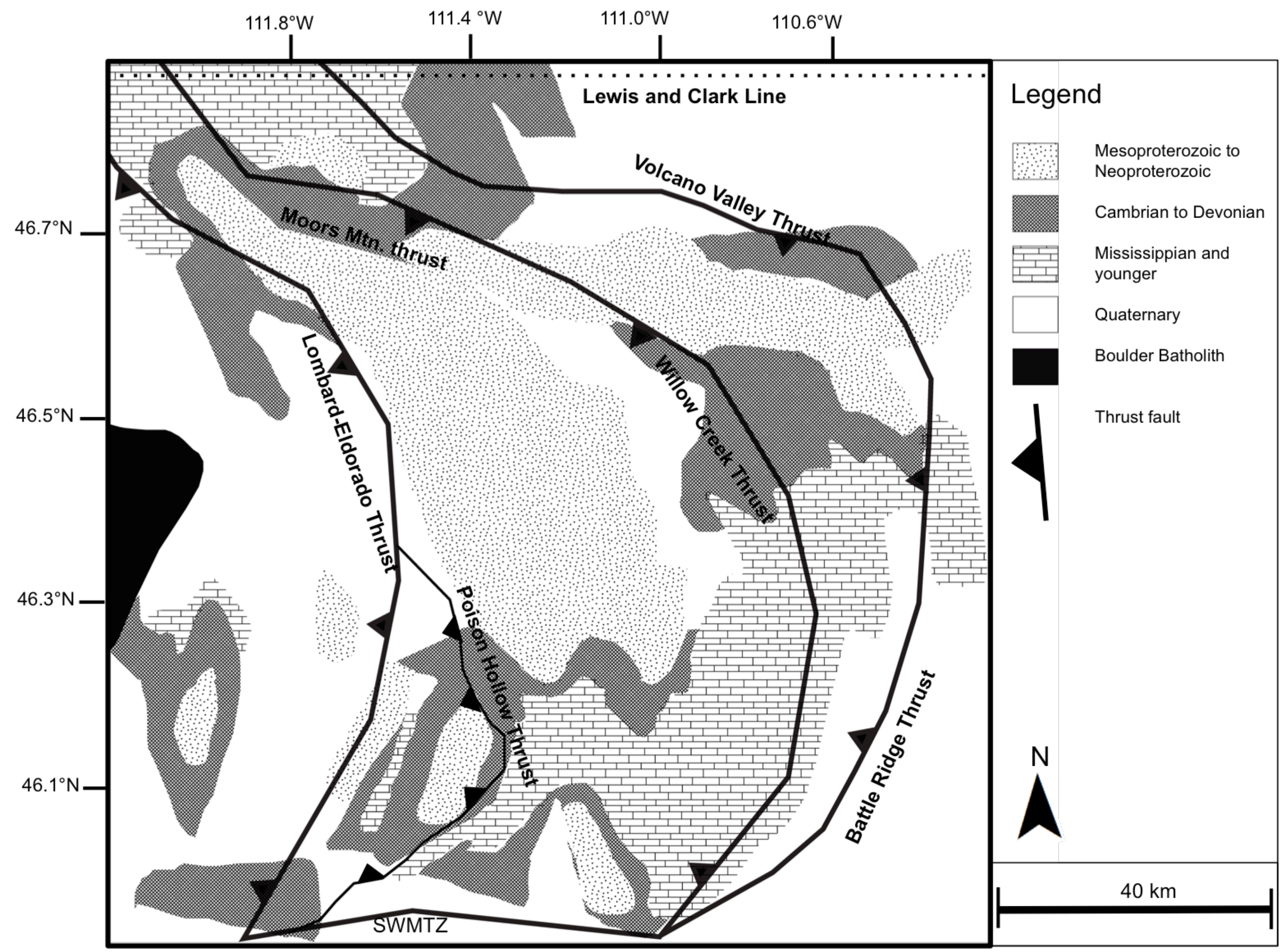

Figure 6: Simplified geologic map of the Helena Salient.

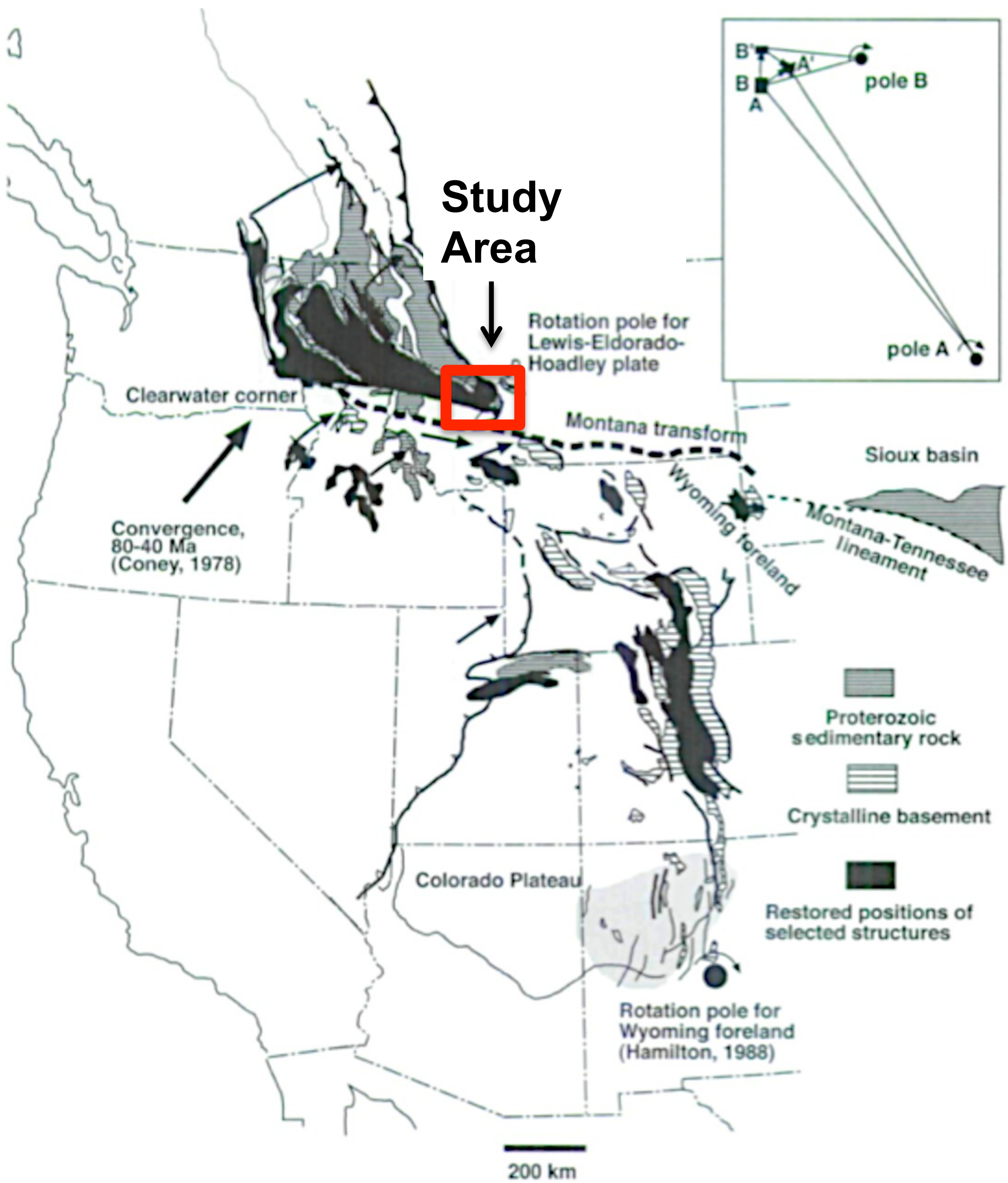

Figure 7: Model for Farallon plate rotation around a pole centered in the Helena Salient based on displacement of Belt-Purcell rocks (Figure modified after Sears, 2006).

3.2 Boundaries of the Helena Salient

Preexisting structures associated with the Belt Basin such as the SWMTZ and LCL that bound the salient (on the south and north) produce complicated interactions between purely thrust-driven deformation and transpressional deformation. The SWMTZ contains anastomosing and imbricated east-verging, north-dipping oblique-slip faults which merge northeastward into the west-dipping thrust faults of the Helena Salient (Schmidt and O'Neill, 1982). As discussed above, the SWMTZ has 20-50 km of right-lateral displacement and is interpreted to be the reactivated southern boundary fault of the Belt Basin (Schmidt and O'Neill, 1982).

The Lewis and Clark Line is another crustal-scale Proterozoic boundary feature that has been active intermittently since the Mesoproterozoic. The Lewis and Clark Line is a Proterozoic structure reactivated in the Late Cretaceous and has an imbricated structure with a maximum slip on the principal faults of up to 28 km based on evidence from lithologic data and outcrop patterns (Wallace et al., 1990).

To the west and south of the Helena Salient are several large intrusive bodies consisting of the Boulder batholith west of the salient and the Pioneer and Tobacco Root batholiths to the south of the salient. The main igneous complex in the Helena Salient is the 6000 km^2 Boulder batholith, which rapidly intruded into the middle to upper crust, within the hanging wall of the Lombard-Eldorado thrust between 80 and 70 Ma (Tilling, 1968, Kalakay et al., 2001, Lageson et al., 2001). The emplacement of the silicic magma of the Boulder Batholith happened at shallow structural levels, implying a rapid emplacement time. Kalakay describes a model in which magma is emplaced along structural anisotropies such as fault zones, which implies the presence of warm lubricating fluids within the major faults of the Helena Salient during deformation (Kalakay et al., 2001). Evidence of this model is found in exposures of the McCartney Mountain thrust salient and the Pioneer Batholith where there is igneous rock in the hanging wall on top of the foot wall indicating ramp-top pluton emplacement.

3.3 Salient Formation

3.3.1 General Salient Models

Numerous models have been proposed to describe the formation of thrust salients and their kinematic evolution. The following sections highlight several possible factors in the kinematic evolution of the Helena Salient as well as the application of other models to the formation of the Helena Salient. The two main types of models, kinematic and dynamic, describe salient evolution using attributes of thrust movement and geometry.

3.3.2 Kinematic Models

Kinematic models of salient formation focus on differences in observed map patterns of deformation to describe salient evolution. Yonkee and Weil (2010) present 4 models to describe the kinematic evolution of a curved orogen (Figure 8). The key differences of these models are parallel versus radial thrusting along with geometric products of the differing thrust trajectories such as rotation and extension.
The predicted observations of these models are arc geometry, vector pattern, and rotation within the limbs.

The two types of arcs, the primary arc and the progressive arc, have geometries dependent on slip pattern and rotation. There are two models illustrating the development of a primary arc salient. The primary arc models both begin as arcs. This arc stays the same size throughout deformation in the uniform slip model but becomes larger throughout deformation in the radial slip model. The primary arc that becomes larger requires a radial displacement pattern towards the foreland, while the primary arc that stays the same size throughout deformation requires parallel translation into the foreland.

The progressive arc bends with its convex side towards the foreland due to differential shortening or divergent emplacement. Both of the progressive arc models require increased curvature throughout deformation and rotation within the limbs. The divergent emplacement arc becomes larger throughout deformation and contains a radial displacement pattern, while the differential shortening arc stays the same size and contains a parallel displacement pattern. Both of the progressive arc models are more complicated than either of the primary arc models due to interactions of rotation and displacement patterns.

3.3.3 Dynamics of Salient Systems

Dynamic salient models enumerate the controls of curved thrust patterns and resultant shortening. The two models presented by Macedo and Marshak (1999), depict the shortening pattern across the salient based on the initial tectonic setting- a basin or an indenter. The basin-controlled model (Figure 9) suggests that wedge taper dynamics and a predeformational basin act together to control the resultant salient geometry (Macedo and Marshak, 1999). The key factor in the basin-controlled model is the spatial distribution (geometry) of the decollement.

A critically tapered Coulomb wedge forms within the extent of the basin-controlled salient with a weak basal detachment between the crystalline basement rock and the overlying predominantly sedimentary formation. The architecture of the predeformational basin is important because it controls the decollement across the salient as the decollement is interpreted to follow the base of the Belt Supergroup. While the wedge moves eastward towards the foreland, the decollement follows the bottom of the formation and ramps up and out of the predeformational basin. The curvature of the salient results from the thick sedimentary packages and shortening is consistent across the salient in a basin-controlled model.

The indenter-controlled model predicts differential shortening across the salient which is caused by a forelandward moving block pushing rock in front of it into an arc shape and as it continues moving into the foreland radial displacement propagates and creates the salient geometry. The indenter-controlled model predicts that shortening is not uniform around the salient; the central section of the salient has the greatest amount of shortening whereas the limbs of the salient have less shortening.

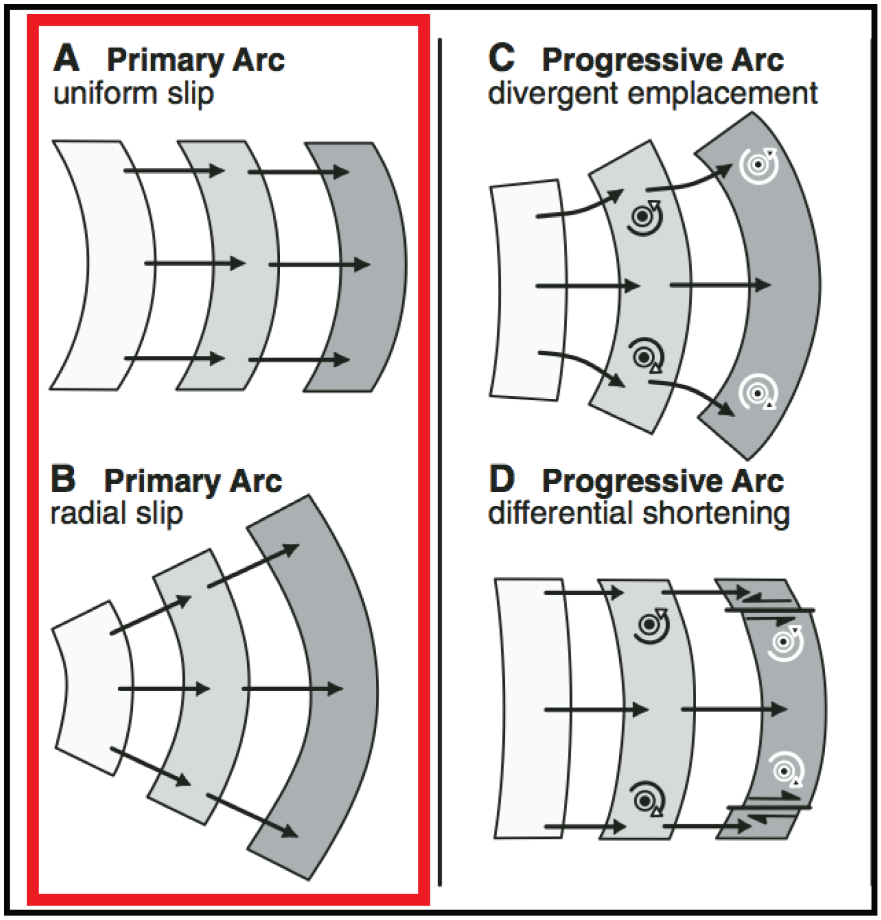

Figure 8: Salient models: kinematic models predicting slip patterns and vector directions as well as rotation (Figure modified after Yonkee and Weil, 2010).

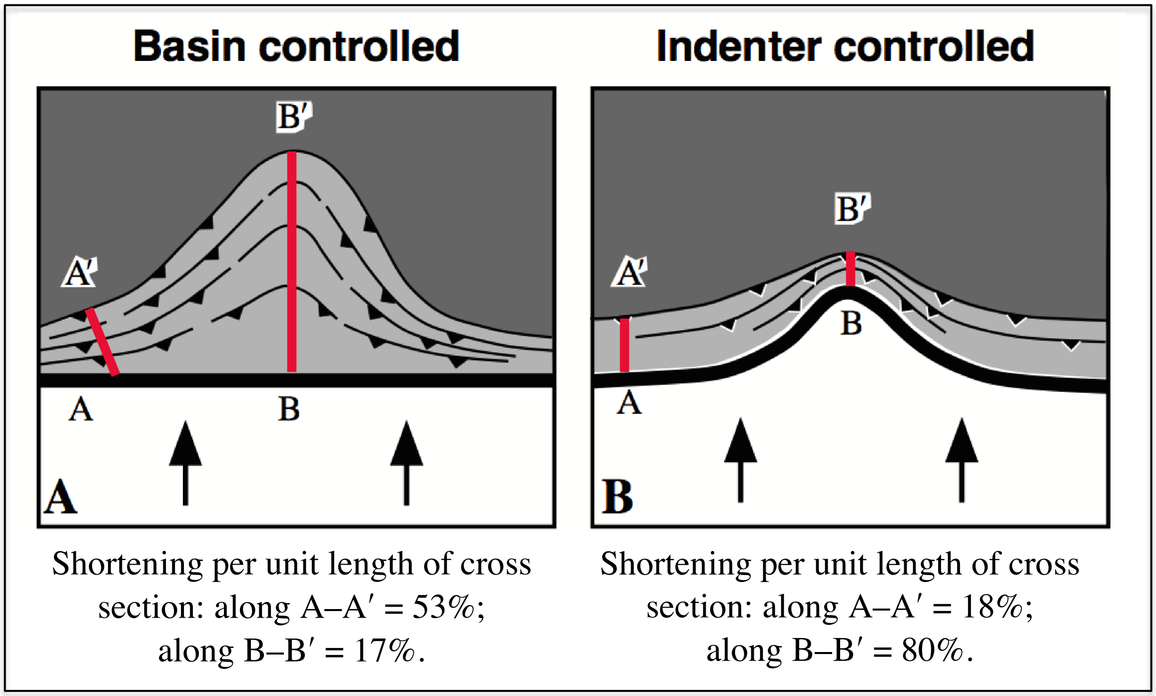

Figure 9: Salient models: basin controlled salient formation and predicted shortening patterns (Figure modified after Macedo and Marshak, 1999).

3.3.4 Formation

General models of salient formation described above can be related to the evolution of the Helena salient in different ways. The basin-controlled model is important due to the presence of the predeformational Belt Basin. The thick Belt Supergroup within the Helena salient provides an important framework for thrust development that may have instigated the formation of radial geometry. Platt and Vissers (1989) describe a similar model in which a laterally tapering wedge instigates radial thrusting that overtime will increase the curvature of the salient.

Mesozoic arc magmatism has been proposed to play a critical role in the development and evolution of the Helena Salient (Lageson et al., 2001). Lageson et al.

(2001) suggests that large volume Late Cretaceous pluton emplacement and volcanism instigated super critical wedge taper conditions that drove thrusting and rapid foreland propagation within the Helena Salient. A key aspect is that the location of arc magmatism spatially and temporally converges with the growth of the Sevier orogenic belt in the region of the Helena Salient as opposed to the north and south of the region where the orogeny evolved in a back-arc foreland setting (Kalakay et al., 2001, Sears, 2006) (Figure 4). Late Cretaceous and early Tertiary calc-alkaline magmatism propagated from the hinterland into the foreland fold and thrust belt concurrent with crustal thickening between 85 and 55 Ma (Kalakay et al., 2001). This is a relatively unique situation of synchronous magmatism and deformation in the North American cordillera. However, this doesn't provide any direct hypotheses to test in regards to the kinematics, and is not discussed further.

4. Kinematic Restorations

4.1 Kinematic Modeling

4.1.1 Methods

Three cross sections were built across the Helena Salient. Section A-A' crosses the northern portion of the salient. Section B-B' follows a direction of the approximate maximum shortening direction as determined by strike and dip data used to produce stereonets in Move (Figure 10). Section C-C' crosses the southern portion of the salient north of the SWMTZ. 2D Move from Midland Valley was used to assist interpretations of structures at depth and to project them above the surface where eroded.

Initial conditions were generalized to apply to all three kinematic models in order to simplify the forward modeling process. For each model, stratigraphic thicknesses are the same and represent a literature-based estimate of thickness in the region. Forward modeling of structures is based on map expressions of the structures and estimated thicknesses in order to produce applicable kinematic models that adhere to surface geology as well as published sections in the region and the accepted subsurface geometry of structures.

A basemap was compiled from USGS geological maps as well as Montana Bureau of Mines and Geology maps (See Appendix 7.2). All surface data: strikes and dips, faults, and map units, were digitized from published geologic maps in the Helena Salient region. The maps were georeferenced in Move; Preliminary Geologic Map of the Townsend 30'x 60' Quadrangle, Montana (Reynolds and Brandt, 2006), Preliminary Geologic Map of the Big Snowy Mountains 30' X 60' Quadrangle (Porter et al., 2005), Geologic Map of the Big Timber 30' X 60' Quadrangle, South-Central Montana (Lopez, 2000), Preliminary Geologic Map of the Bozeman 30' x 60' Quadrangle Southwestern Montana (Vuke et al., 2002), Geologic Mao of the Canyon Ferry Dam 30' x 60' Quadrangle, West-Central Montana (Reynolds and Brandt, 2006), Geologic Map of the Livingston 30' x 60' Quadrangle, South-Central Montana (Berg et al., 2000), Preliminary Geologic Map of the White Sulphur Springs 30' x 60' Quadrangle, Montana (Reynolds and Brandt, 2007), Geologic Map of the Harlowton 30' x 60' Quadrangle, Central Montana (Wilde and Porter, 2008), Preliminary Geologic Map of the Ringling 30' x 60' Quadrangle, Central Montana (McDonald et al., 2005).

The geologic basemap and all other data were geo-referenced using Move software. A DEM from the USGS was draped over the geologic basemap to produce a 3D map of current day geology and topography. Strike and dip data were collected and digitized as well as important geologic horizons and structures, in order to build the models and sections. Figures 10 and 10B depict stereonet diagrams, which were used to choose the locations of the three cross sections produced in this study. Section orientation was determined from stereonet data as well as literature-based estimates of the maximum shortening direction derived from published regional sections within the Helena Salient. (See Appendix 7.1 for all strike and dip data). The stereonets in Figure 10B were created using Move's section orientation algorithm; it compiles a specified cluster of strikes and dips within proximity of the cross section and projects these points onto the stereonet. From the stereonet data, it draws a line of best fit determined by concentrations of strikes and dips on the stereonet that reflect an approximate perpendicular orientation to the regional strike of bedding.

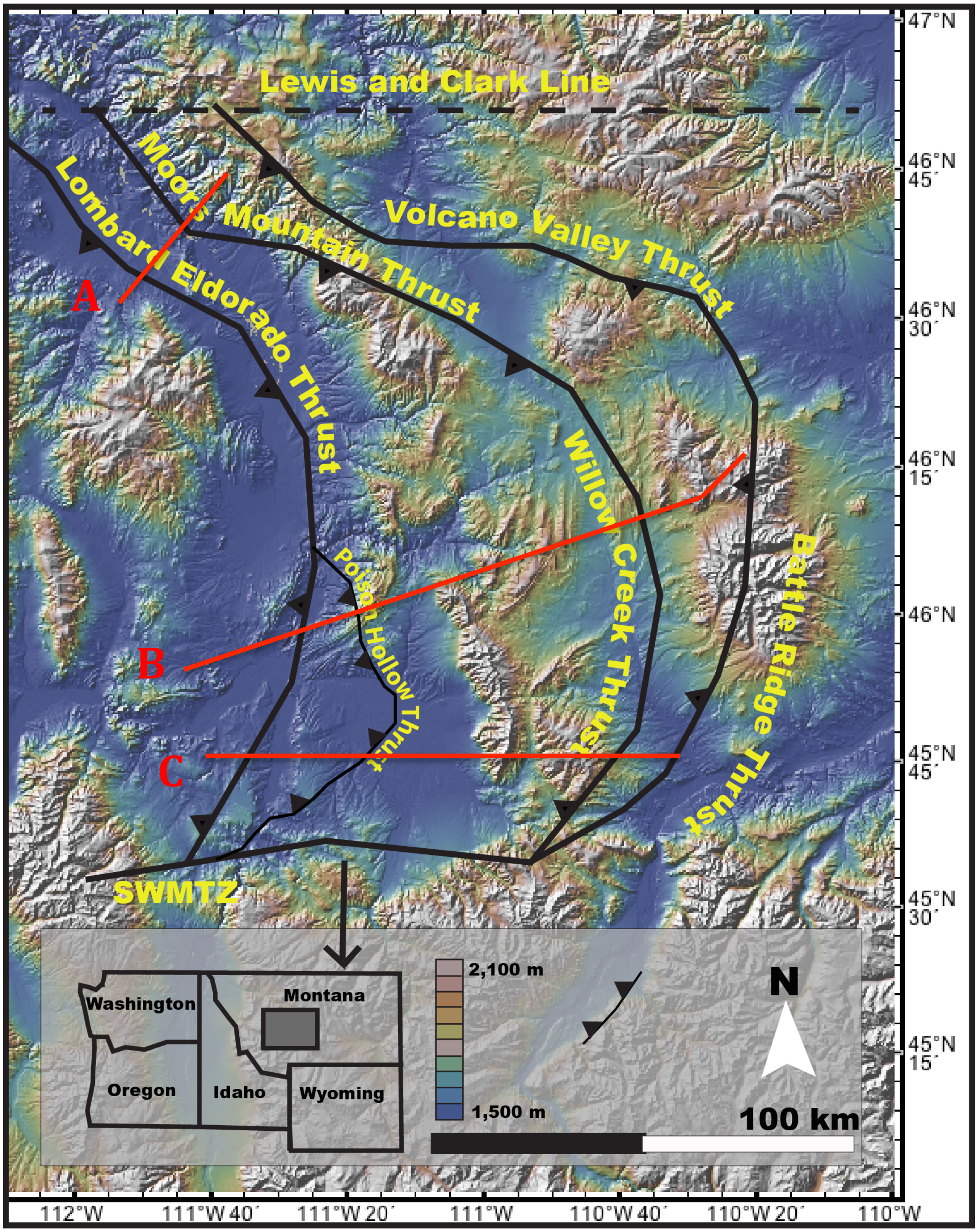

Figure 10: Locations of the three cross sections produced in this study were chosen based on regional interpretations of strikes and dips using Move software. Stereonets from the three sections, A, B, and C, are displayed in Figure 10B.

A

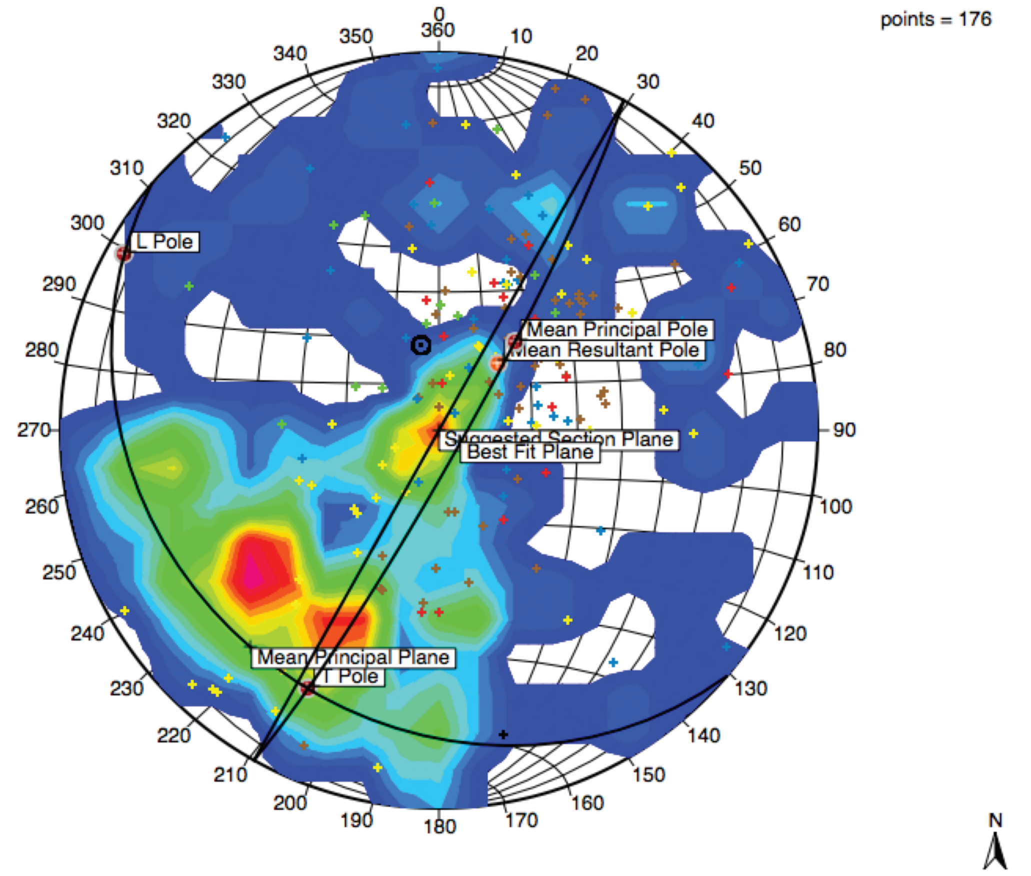

B

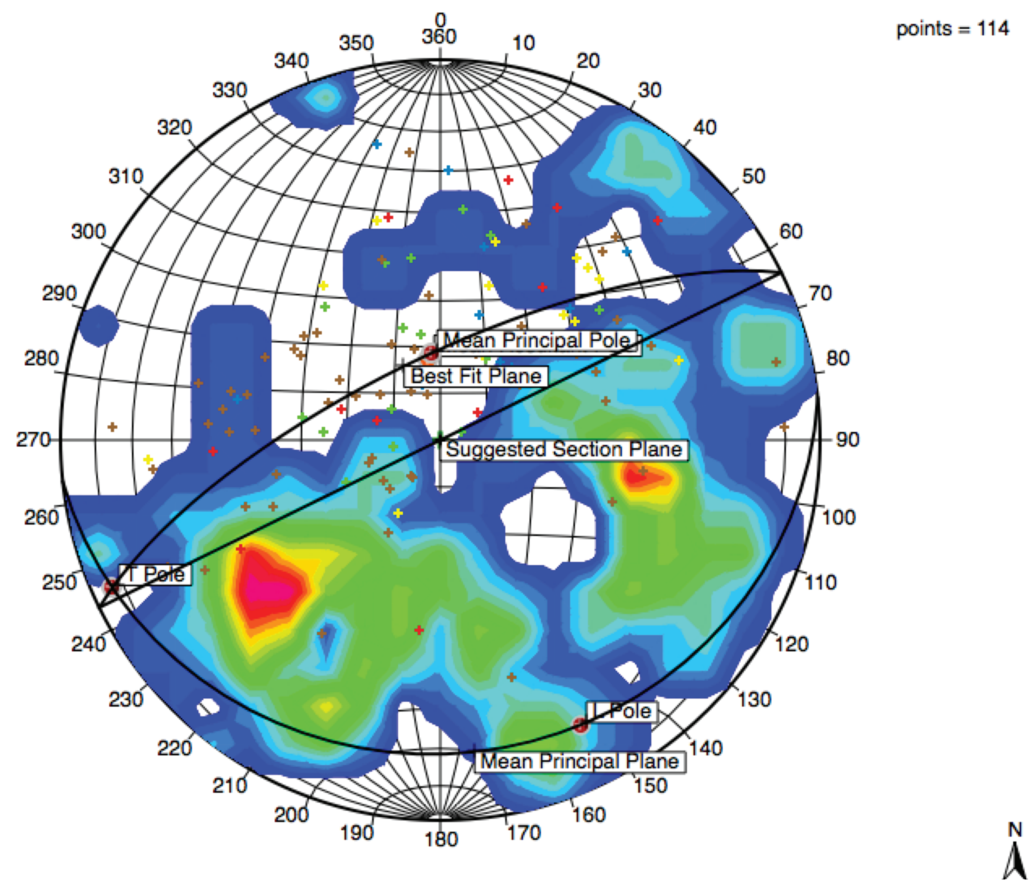

C

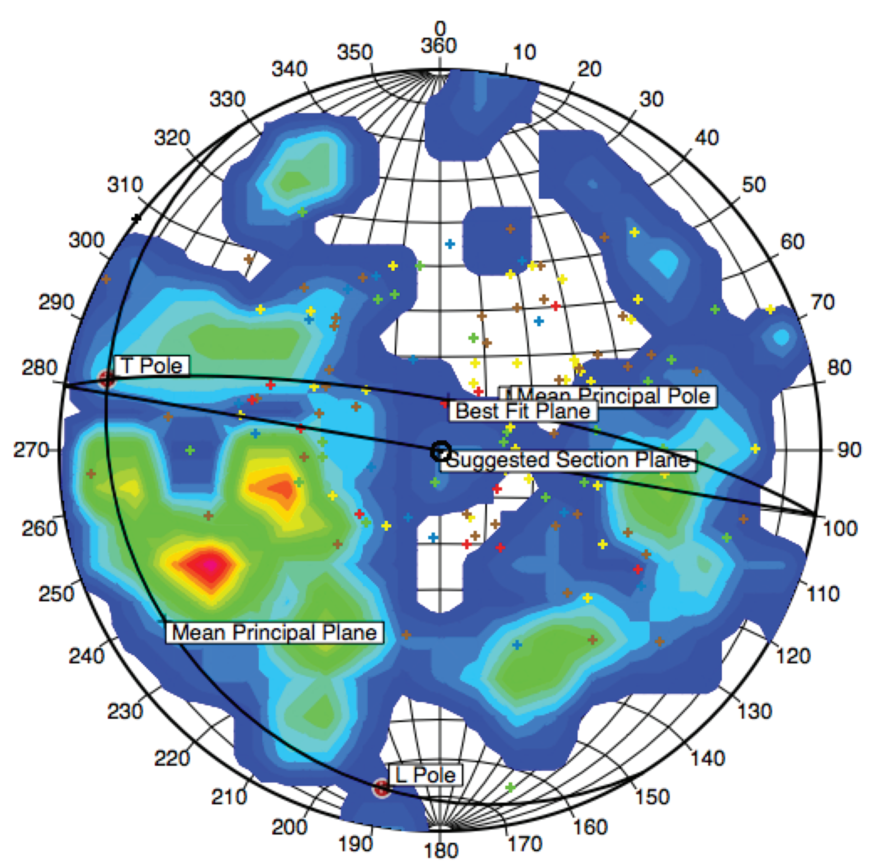

Figure 10B: Displayed are the mean principal pole, the mean resultant pole, the L pole (beta-axis), the T pole, the mean principal plane, the best fit plane and the suggested section plane. The color map represents dip directions. Red is a maximum dip direction and blue is the minimum dip direction. Move's algorithm determines the section orientation line as discussed in section 4.1.1.

4.1.2 Assumptions and Uncertainty

The kinematic models presented in this paper represent possible solutions to the evolution of large-scale structures and regional cross sections. The following models are meant to depict the major thrust faults of the Helena Salient, the LET, MMT, and the VVT. These solutions are based on known assumptions:

1. Plane strain is modeled as the principle mechanism of deformation and therefore shortening occurs in the direction of the cross sections only.
2. Thickness of rock formations is modeled as homogenous across the Helena Salient. Thickness data are determined from map orientations as well as a literature-based review.
3. The three algorithms used to build forward models in 2D Move are; fault propagation folding, fault bend folding, and the unfolding tool. Based on the modeled units and the forward modeling tools, small structures in the area have not been accounted for.
4. The published geologic maps provided all data and models assume accuracy of the data.

4.2 Forward Model A-A’

4.2.1 Cross Section A-A’

Folds and thrust faults along the cross section verge north-east (see geologic map: Appendix 7.2). The inferred decollement above the Proterozoic crystalline basement is based on previously published sections as well as other structural interpretations by Lageson (2001), DeCelles (2004), and Sears (2006). The key elements from southwest to northeast are the LET, the MMT, the antiformal structure, and finally the klippe (Figure 11) The LET places Proterozoic units on top of Cambrian units, the MMT places Proterozoic units on top of Cretaceous units, and then the antiformal structure is bound by the MMT, which places a Proterozoic klippe on top of the Cretaceous rock at the end of the section.

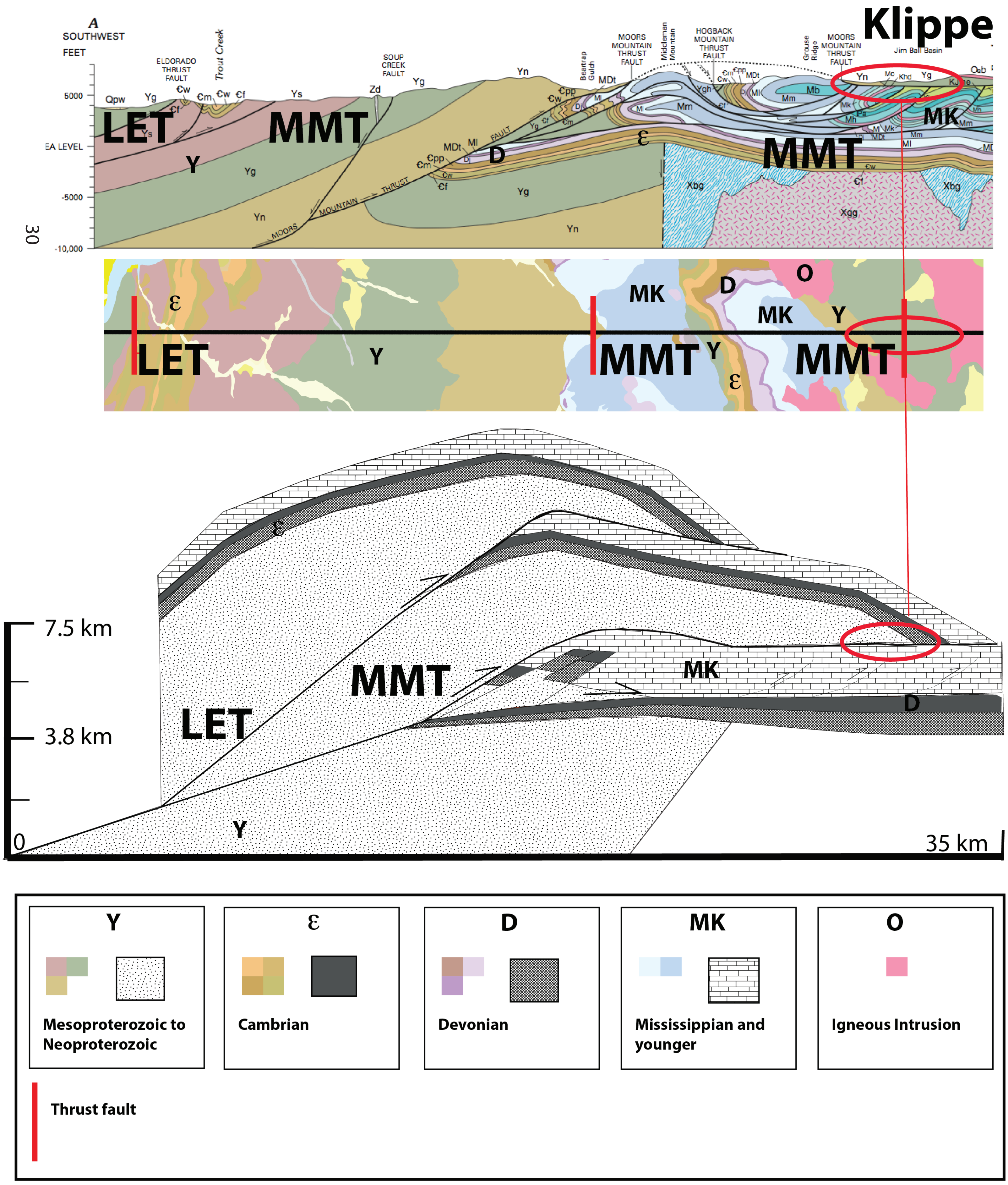

Figure 11: Section A-A' was built using 2D Move. From top to bottom: Reference cross section, strip map with modeled section line, modeled section (Reynolds and Brandt, 2006).

4.2.2 Kinematics

Forward model A (Figure 12) shows the structural evolution of cross section A-A' (Figure 11). Figure 12A consists of an undeformed succession of Mesoprotorozoic, Cambrian, Devonian, Mississippian, Cretaceous and younger sediments along the northern boundary of the Belt graben where the Mesoproterozoic Belt Supergroup sediments end. The northern margin of the Belt Basin which juxtaposes crystalline basement rock in section A-A' was interpreted by published sections and Sears' palinspastic reconstruction of the Belt Basin (Sears, 2007) (Figure 3).

There is 6.3 km of shortening by the LET from the regional detachment which ramps up through the Belt Basin rocks and places the Belt Basin rocks on top of the Cretaceous and younger packages (12B). This shortening is modeled as a fault with a fault bend fold in the hanging wall. Deformation propagates into the foreland with 8.5 km of shortening on the MMT (12C). The MMT places Belt Supergroup strata on the Cretaceous and younger strata. As these two large sheets move to the northeast, imbrication of the Phanerozoic succession occurs above the regional decollement at the bottom of the Phanerozoic sequence (Figure 12D).

An antiformal duplex of Belt Supergroup through Cretaceous sediments forms between the MMT and the Phanerozoic base. This portion of the model is based on a hypothetical deformation process illustrated in the reference cross section and is meant to represent the feasibility of a structural high in this portion of the section as opposed to representing a plausible mechanism of formation. Deformation along the decollement is transferred to the MMT resulting in their hanging walls overthrusting Phanerozoic sequences. This is produced by out-of-sequence thrusting evidenced by deformation and erosion of underlying units prior to the emplacement of the Belt Supergroup klippe. Displacement of the LET and the MMT continues into the foreland with 10.2 km of shortening. The fault-bend folds relating to this step are placed at the end of the section in order to represent the possible deformation of smaller structures in the section, not to represent a quantifiable amount of shortening due to the formation of these structures. According to the east-dipping beds of the klippe and the west-dipping folds of the underlying Phanerozoic units, folding of the Cretaceous and younger units occurred prior to emplacement of the Belt Supergroup klippe.

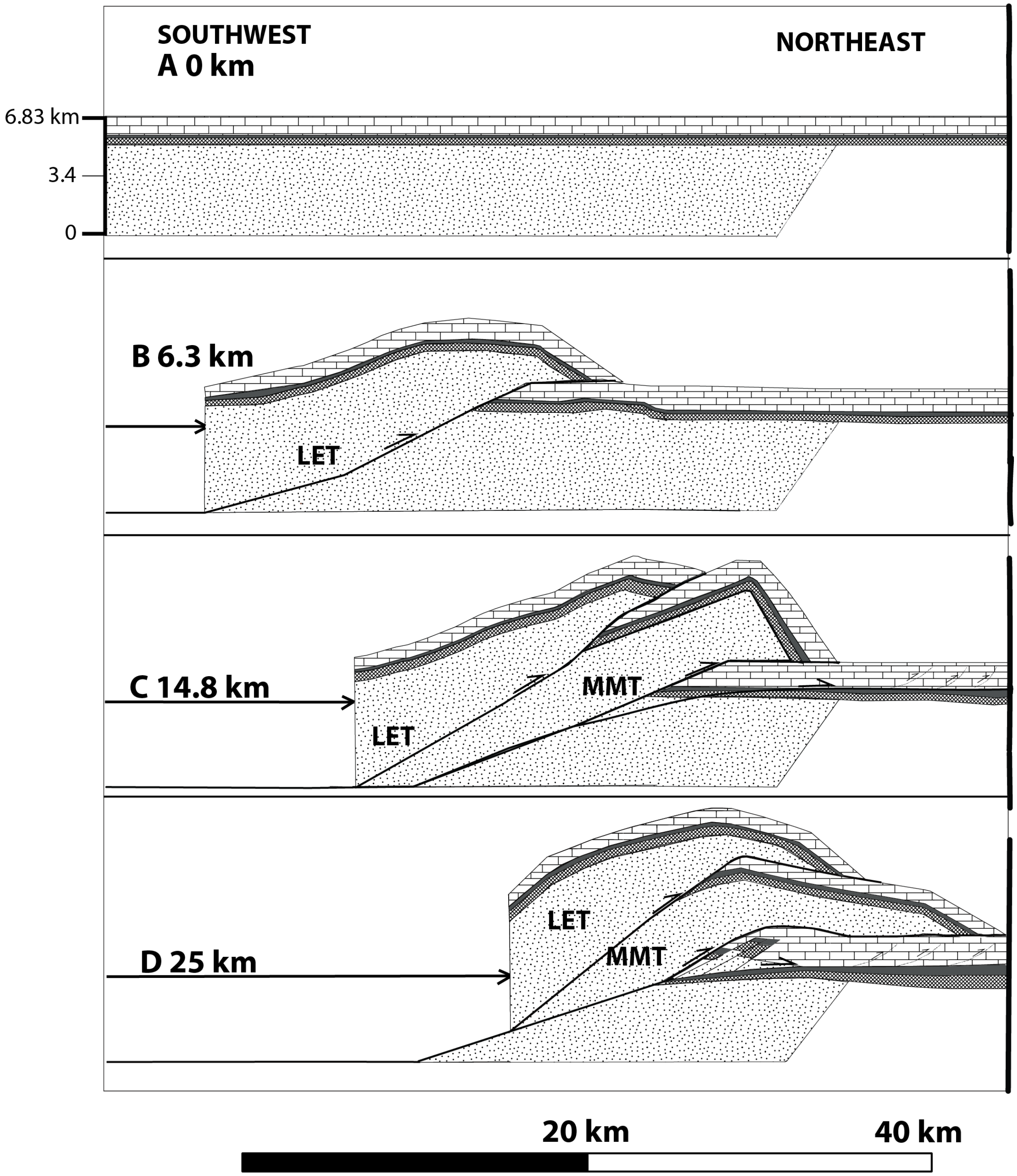

Figure 12: Forward model of section A-A'.

4.2.3 Shortening

Shortening was measured in each step of the model. The model steps correspond with the displacement of the major thrusts in the system the LET and the MMT. A cumulative estimate of the magnitude of shortening from Figure 12A to 12B is 6.3 km- corresponding with LET displacement. The magnitude of shortening from figure 12B to 12C is 8.5 km, which corresponds with displacement of the MMT. The magnitude of shortening from Figure 12C to 12D is 10.2 km. The total amount of shortening in section A-A' is 25 km.

4.3 Forward Model B-B'

4.3.1 Cross Section B-B'

Structures of the cross section are east verging (see geologic map: Appendix 7.2). The inferred decollement above the Proterozoic crystalline basement is based on previously published sections as well as other structural interpretations by Lageson (2001), DeCelles (2004), and Sears (2006). The key elements from west to east are the LET, the PHT, the MMT, fault propagation folding, and the VVT (Figure 13). The thrusts are in-sequence starting with the LET and then the PHT, followed by the MMT and finally the VVT, which is a blind thrust. Propagation folding between the MMT and the VVT occurs after initiation of the MMT and before/during initiation of the VVT.

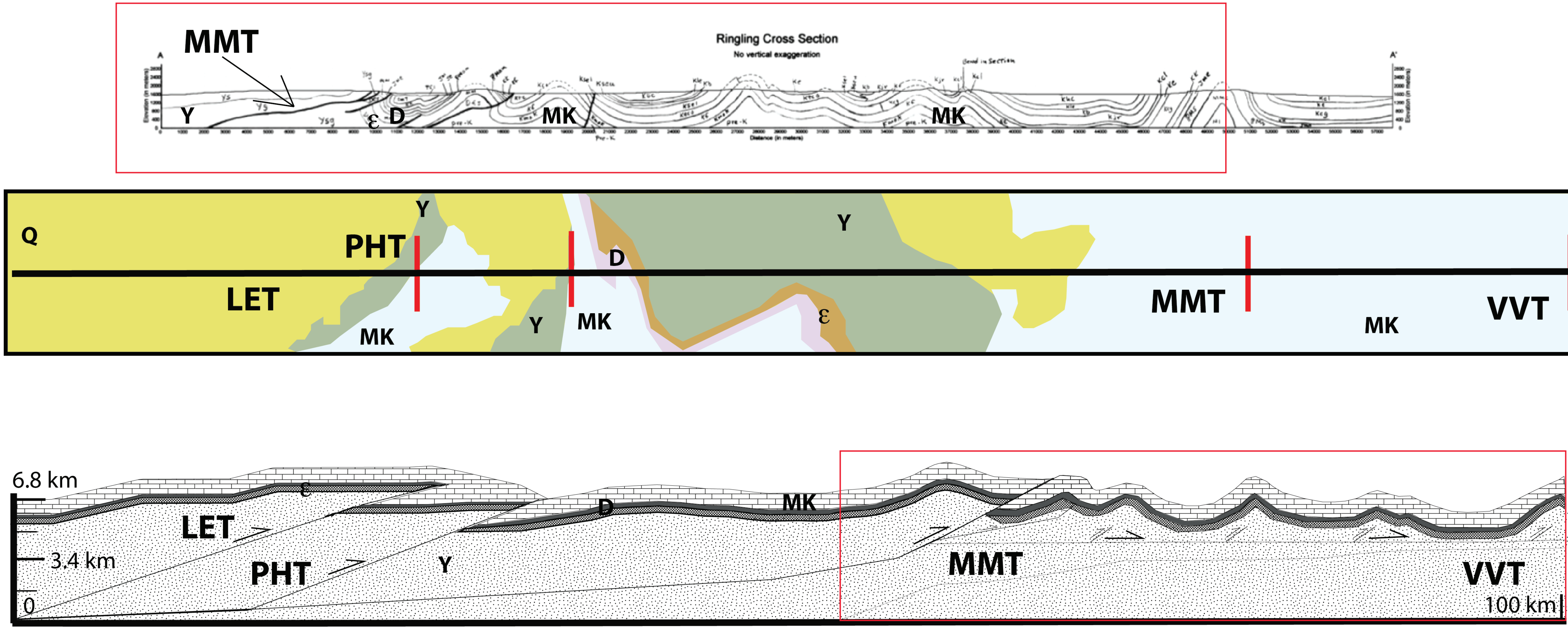

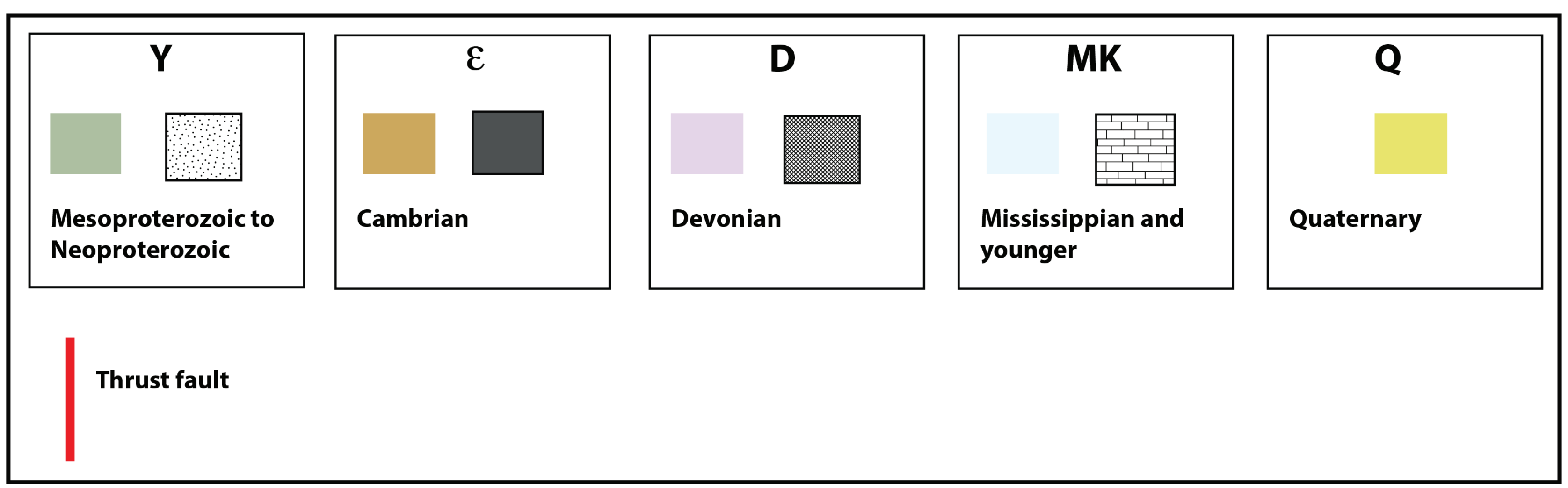

Figure 13: Section B-B' was built using 2D Move. From top to bottom: reference section, strip map with modeled section line, and modeled section (McDonald et al., 2005,Reynolds and Brandt, 2006.)

4.3.2 Kinematics

Forward model B (Figure 14) depicts the structural evolution of this cross section (Figure 13). Cross section B is located in the middle of the salient (Figure 10). The decollement is placed above the Proterozoic crystalline basement based on previously published sections as well as other structural interpretations by Lageson (2001), DeCelles (2004), and Sears (2006). The LET and PHT ramp up and over the Phanerozoic sequences placing Belt Supergroup over the Phanerozoic sequences (Figure 14B). There is 8 km of shortening from the regional detachment along the top of the Proterozoic crystalline basement. This shortening is modeled as fault propagation folding in the foreland.

Displacement along the regional decollement continues into the foreland as the MMT places Devonian strata on top of Cambrian strata (Figure 14C). The MMT continues east into the foreland with fault propagation folding from movement on thrusts, activating the VVT, which is modeled as a blind thrust system (Figure 14D).

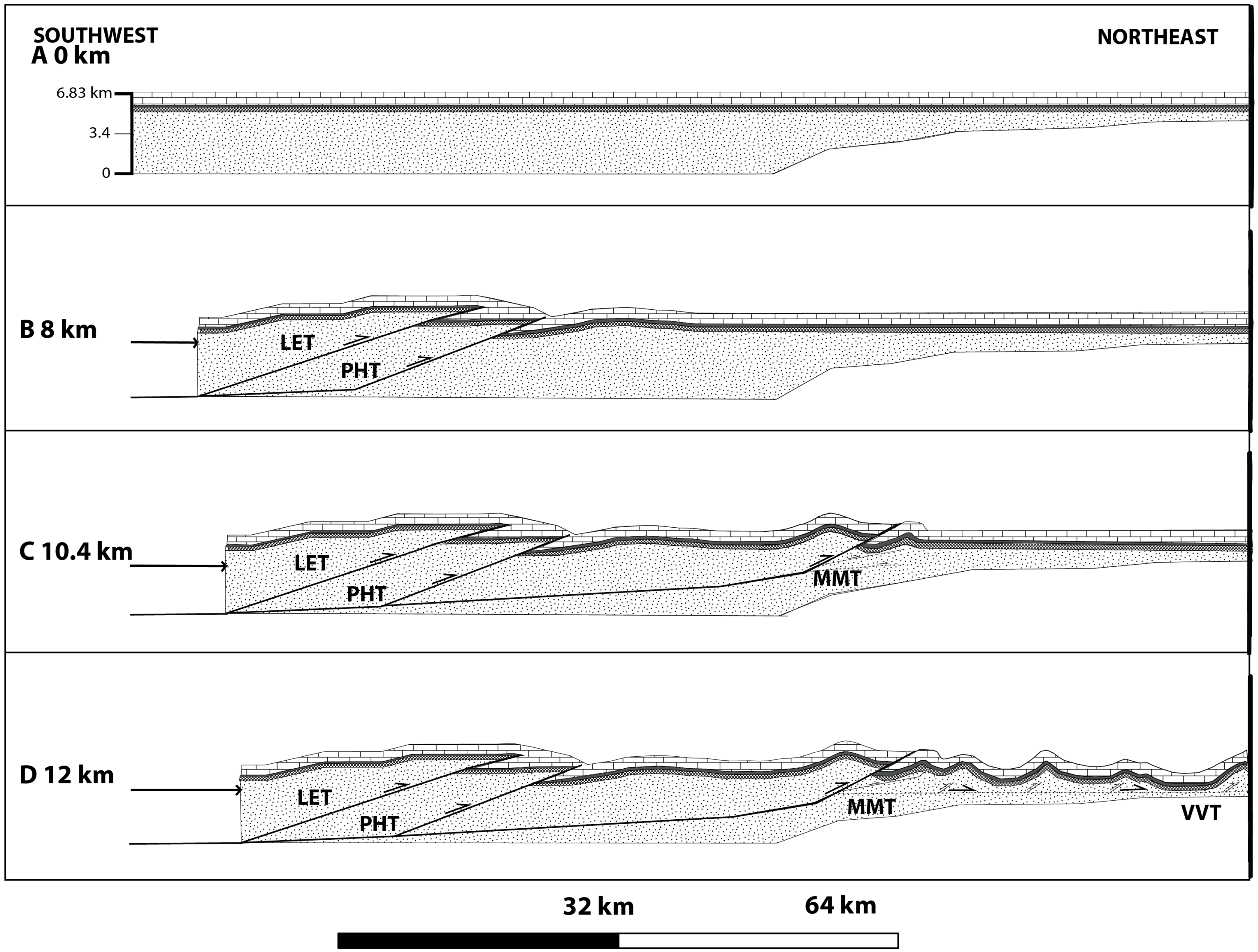

Figure 14: Forward model of section B-B’.

4.3.3 Shortening

Shortening was measured in each step of the model. The model steps correspond with the displacement of the major thrusts in the system the LET, MMT, and the VVT. Cumulative magnitude of shortening from Figure 14A to 14B is 8 km. This estimate of shortening corresponds with displacement of the LET. The magnitude of shortening from Figure 14B to 14C is 2.4 km. This estimate of shortening corresponds with displacement of the MMT. The magnitude of shortening from Figure 14C to 14D is 1.6 km. This displacement corresponds with the VVT. The total amount of shortening in section B-B' is 12 km.

4.4 Forward Model C-C'

4.4.1 Cross Section C-C'

Structures of the cross section are east verging (see geologic map: Appendix 7.2). The inferred decollement above the Proterozoic crystalline basement is based on previously published sections as well as other structural interpretations by Lageson (2001), DeCelles (2004), and Sears (2006). The key elements from west to east are the LET, PHT, fault-bend folding, the MMT and the VVT (Figure 15). The thrusts are in sequence beginning with the LET, the PHT, the MMT and finally the VVT.

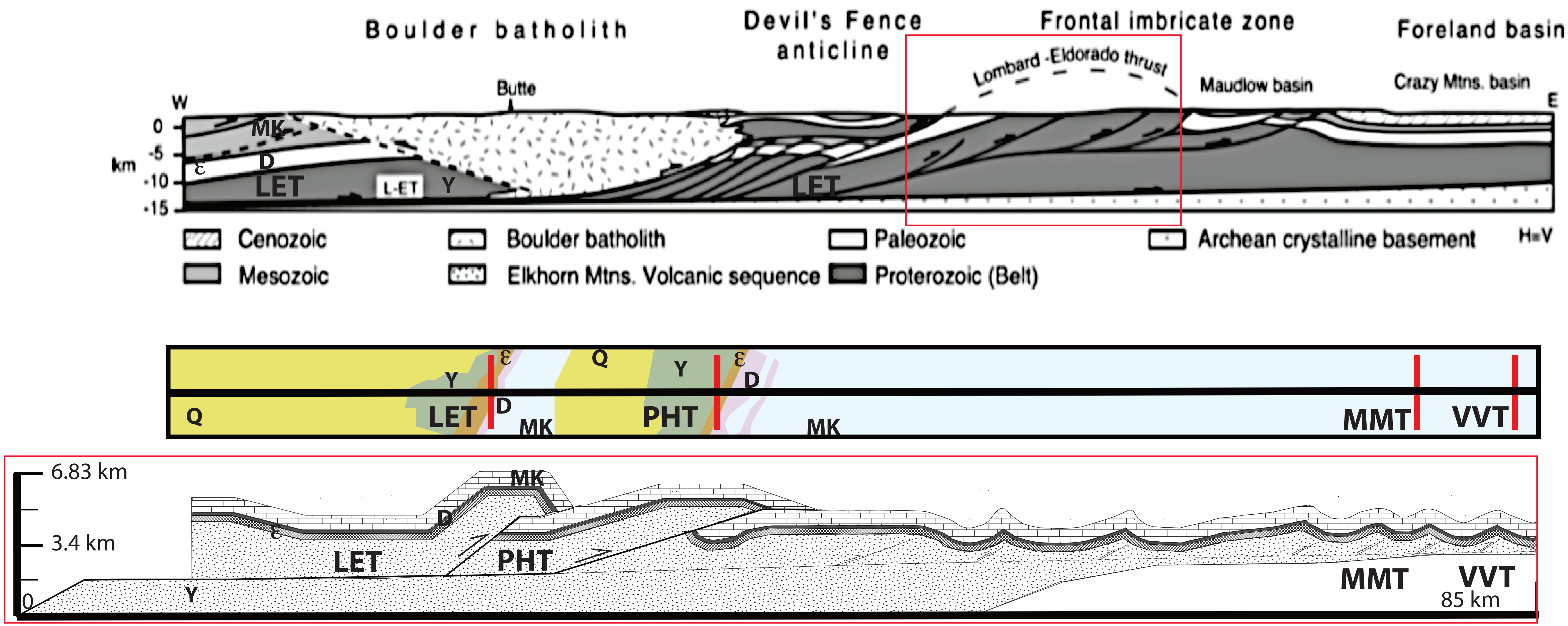

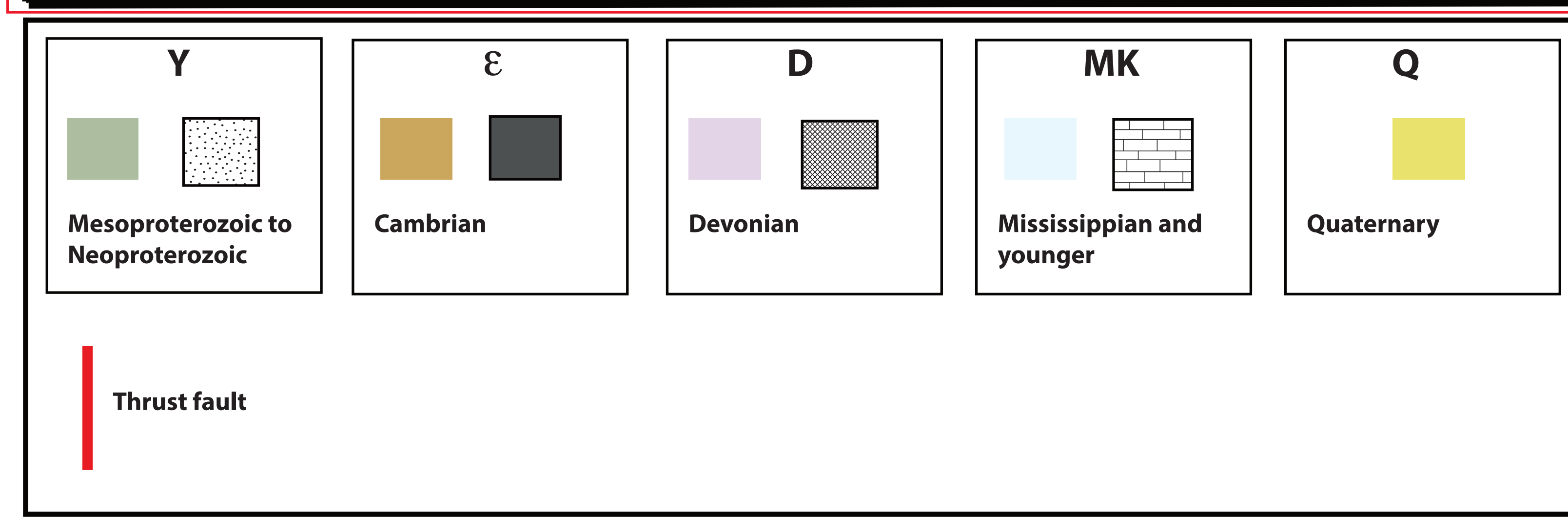

Figure 15: Section C-C' was built using 2D Move. From top to bottom: reference section, strip map with modeled section line, and modeled section (McDonald et al., 2005, Reynolds and Brandt, 2006, Lageson et al., 2001.)

4.4.2 Kinematics

Cross section C (Figure 15) occurs along the southern margin of the Helena Salient sub-parallel to the SWMTZ. The undeformed section consists of Mesoproterozoic, Cambrian, Devonian, Mississippian, Cretaceous, and younger rocks. While the Belt Basin's trough cores the salient and becomes shallower to the northeast, the Belt Supergroup is modeled to have the same thickness as section A-A' in order to simplify the modeling process. This is consistent with other published sections in the area and represents a plausible geometry based on surficial geological elements (Lageson et al., 2001, McDonald et al., 2005, Reynolds and Brandt, 2006). Figure 16B shows the initiation of the LET system, which propagates east toward the foreland and ramps up and out of the Proterozoic rocks of the Belt Basin placing the Belt Basin rocks over the Cretaceous and younger rocks. The fault-bend fold morphology was chosen because of the map-view shape of the fold consisting of Proterozoic Belt Basin rocks, which is large and wide.

As deformation propagates east, the PHT initiates 8 km of shortening along the regional detachment placing the Belt Basin rocks over the Cretaceous and younger rocks in a similar configuration as the LET (16C). Figure 16D shows additional displacement on the decollement and initiation of the VVT, 0.5 km of shortening is compensated by thin-skin deformation propagating into the foreland as folds result from blind thrusts above the decollement.

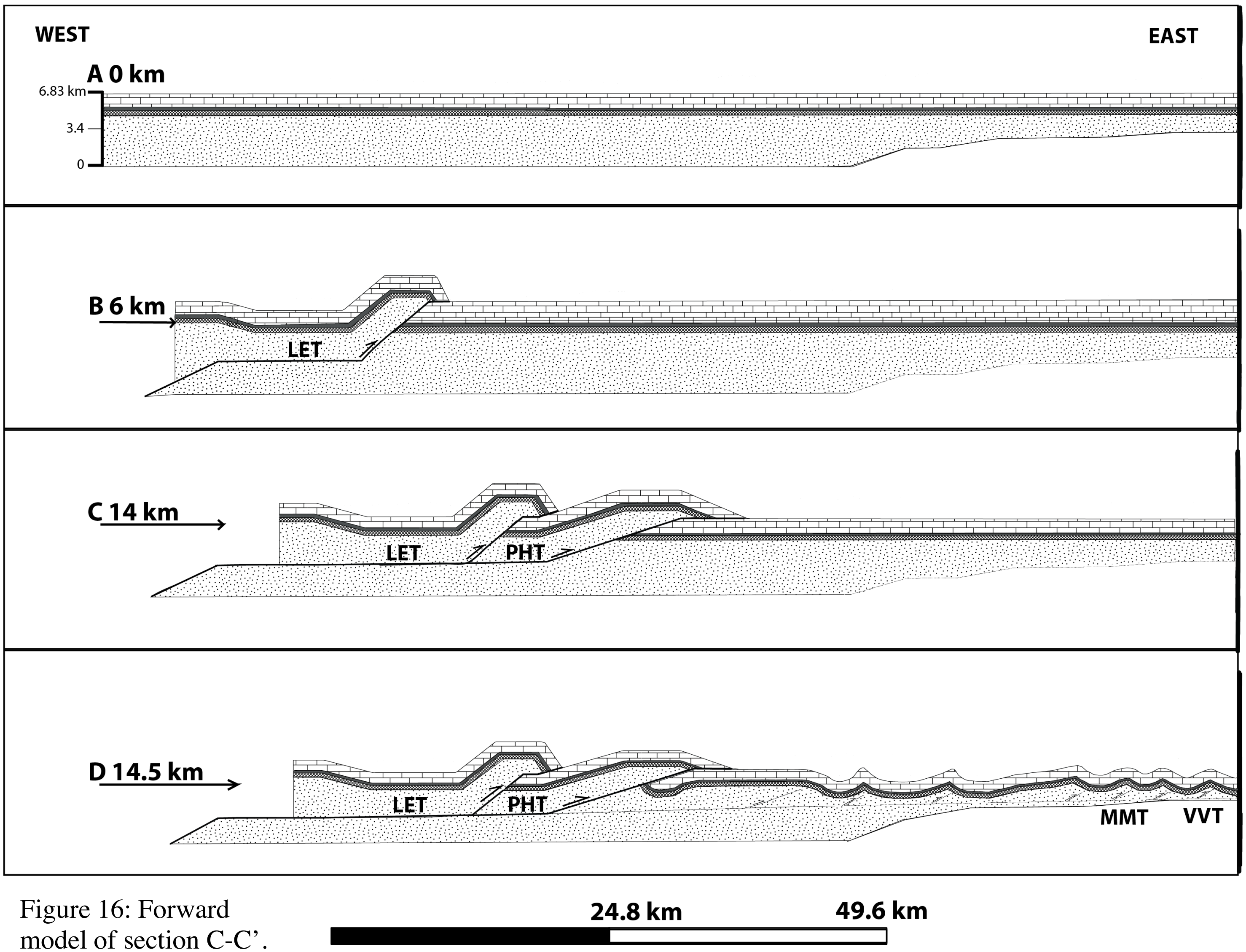

Figure 16: Forward model of section C-C'.

4.4.3 Shortening

Shortening was measured in each step of the model. The model steps correspond with the displacement of the major thrusts in the system the LET, MMT, and the VVT. A cumulative estimate of the magnitude of shortening from Figure 16A to 16B is 6 km, corresponding with displacement of the LET. The magnitude of shortening from Figure 16B to 16C is 8 km displacement on the MMT. The magnitude of shortening from Figure 16C to 16D is 0.5 km of displacement of the VVT. The total amount of shortening in section C-C' is 14.5 km.

5. Interpretations and Discussion

5.1 Shortening

Table 1 shows calculated estimates of total shortening for the major fault systems within the Helena Salient compared to published estimates of region specific shortening. Forward model A has the greatest amount of shortening (25 km). The second largest amount of cumulative shortening occurs in forward model C (14.5). The forward model of section B-B' has the least amount of shortening (12 km).

Shortening estimates agree with published calculations (Bregman, 1976, Schmidt and O'Neill, 1982, Schmidt, 1983, McMechan and Thompson, 1993, Lageson et al., 2001). There are two categories of published estimates; LET shortening, and shortening within the regional extent of this study. The estimate of shortening unique to the LET is from the Lageson (2001) study, which estimates up to 200 km of shortening in the northern US Rockies and southern Canadian Rockies due to the LET. This estimate accounts for the structure over a much broader region and is not useful for evaluating shortening in the Helena Salient because of the focus of this study on structures within the salient. McMechan and Thompson (1993) describe at least 165 km of total shortening in northwestern Montana, around the northern border of the Helena Salient. There is a minimum estimate of 15 km of shortening east of the Boulder Batholith (Schmidt, 1983) and a maximum of 17 km of displacement of the LET near the SWMTZ (Bregman, 1976). Displacement along the southern boundary of the SWMTZ is at least 15 km (Schmidt and O'Neill, 1982).

The observed shortening pattern deviates from the predictions of the general salient models: there is a high magnitude of shortening in forward model A that differs from the predicted shortening pattern of consistent along-strike shortening. The basin-controlled model and the primary arc parallel translation model predict the same amount of along-strike shortening throughout the salient.

Total Shortening

Forward Model A	**Forward Model B**	**Forward Model C**
25 km	12 km	14.5 km
Schmidt (1983)	**Lageson (2001)**	**Bregman (1976)**
>15 km of shortening east of the Boulder Batholith	>200 km of shortening in the northern US Rockies and southern Canadian Rockies	<17 km displacement of the LET

Table 1: Calculated shortening compared with published shortening estimates in the Helena Salient.

5.2 Finite Displacement Model

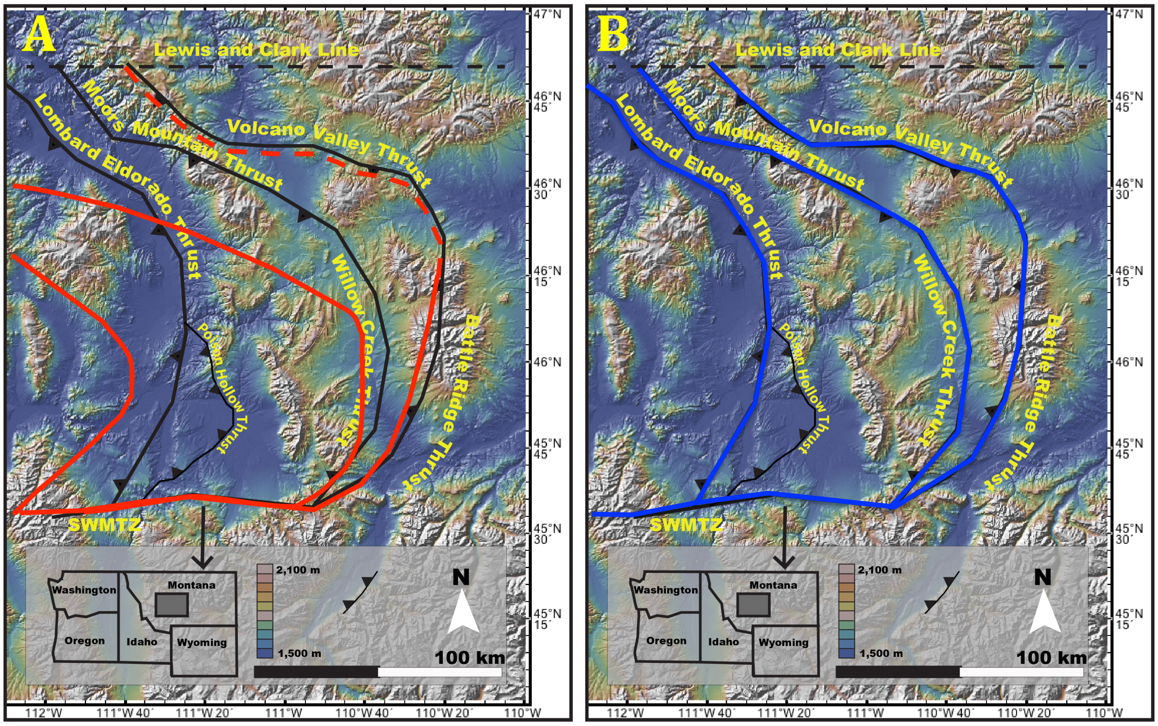

Figure 17: The finite displacement model of the Helena Salient contains Diagram A on the left and Diagram B on the right. Diagram A displays red lines, which are the restored fault traces, and black lines, which are the current fault traces. Diagram B on the right displays blue lines, which represent current day fault traces.

This finite displacement vector model is based on the stepwise shortening produced by the three major thrust faults, constructed by using the calculated estimate of total shortening on each section and pulling the current day thrusts back to the estimated initial location of thrusting. The dashed line in diagram 17A indicates the predicted location of the VVT, as it was not calculated in this study. The finite displacement model displays the along-strike differences in shortening magnitude; the northern portion of the salient has undergone more shortening than the southern portion of the salient.

The geometry of the map-view thrusts in the southern portion of the salient appears to fit closely with model A from Yonkee and Weil (2010) which requires uniform slip, while the northern portion of the salient appears to require radial slip, similar to model B from Yonkee and Weil (2010) (Figure 8). The primary arc with radial slip or uniform slip models implies uniform shortening around the salient according to the models of Yonkee and Weil (Figure 8). Comparing the initial and current day geometries of the thrust faults within the salient indicates a uniform deformation pattern in the south while the northern portion of the salient deviates from the predicted model of uniform shortening.

The model provides evidence that the kinematic evolution of the salient is not as simple as a basin-controlled model or a single vector model from Yonkee and Weil (2010). The basin-controlled model insinuates that total shortening is uniform around the salient, which is inconsistent with the findings of my study. The finite displacement model shows the southern portion of the salient having undergone uniform slip while the northern portion appears to have undergone radial slip. This deviation in slip patterns may be accounted by rotation as discussed in section 5.2.2.

5.2.1 Belt Basin

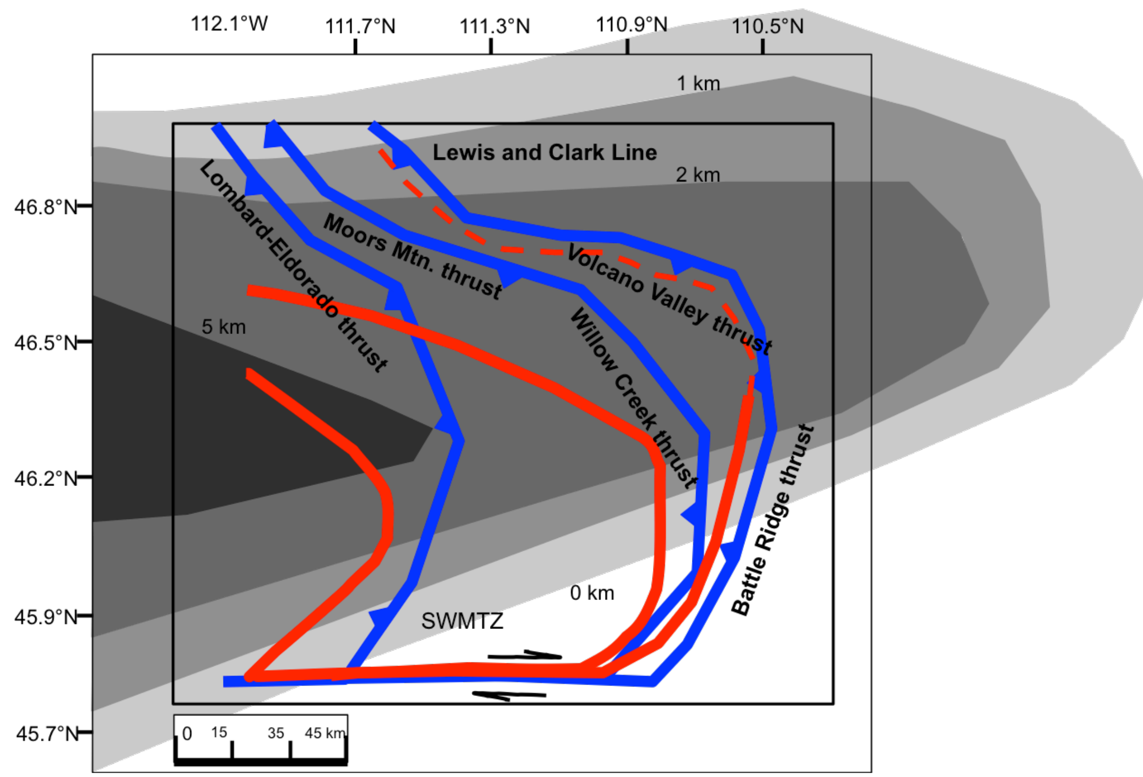

Figure 18: Finite displacement model superimposed on an isopach map (in gray) of the restored lower Belt Supergroup formation (Adapted from Price and Sears, 2000). Red lines are restored fault lines and blue lines are current day traces of faults.

Figure 18 displays the restored-extent and thickness of the reconstructed Lower Belt Basin overlain with the current and restored thrust sheets. The thickness variation and trough axis of the basin illustrate its likely kinematic control over the formation of the salient. The Helena Salient probably started as a primary arc due to the differential sediment thickness of the Belt Basin and the three dimensional shape of the predeformational Belt Basin likely controlled critical taper conditions as the decollement within the salient is interpreted to bound the bottom of the Belt Basin.

The key to the basin-controlled model is the location of the weak detachment because this determines wedge-taper conditions. The decollement depth follows the bottom of the predeformational basin and as the basin becomes shallower and eventually nonexistent, the decollement becomes shallower and mimics the shape of the predeformational basin. The height and width of the thrust wedge is proportional to the depth to detachment and as the depth becomes more shallow the width of the wedge decrease to maintain critical taper (Marshak and Wilkerson, 1997). The wedge taper within the Helena salient is dependent on the three-dimensional shape of the predeformational Belt Basin in that the depth to detachment is the deepest in the trough of the basin and the wedge thickness is the greatest. Likewise, wedge decreases as the basin becomes shallower. This interaction between basin thickness and wedge taper dynamics created the arcuate geometry of the Helena Salient. The nature of the decollement and three-dimensional architecture of the Belt Basin was the primary driver of the formation of the salient. The basin-controlled Helena Salient began as an arc suggesting that a combination of models A and B from Yonkee and Weil (2010) (Figure 8) is applicable to describe the salient's formation.

5.2.2 Rotation

The rotation model shows the interaction of shortening and block rotation within the Helena salient based on the Sears (2006) study and the results of this study (Figure 19). The model depicts different magnitudes of shortening caused by two different pole locations and two different amounts of rotation. The location of the pole is critical to shortening magnitudes and vector directions across the salient. The two pole locations of Figures 19A and 19B compare the suggested pole location of Sears (2006) in Figure 19A to a plausible pole location in 19B. Figure 19A conflicts with the models of this study because it suggests a west-vergent sense of motion in the southern portion of the salient. If the pole is moved near the SWMTZ, clockwise motion throughout the salient remains north-eastward to eastward, which agrees with the vector directions of the finite displacement model as well as the sense of motion on the northern (Lewis and Clark Line) and southern (SWMTZ) borders of the Helena Salient. This pole location contributes to differential shortening across the salient, as it indicates up to 40 km of rotation near to the location of cross section A. Cross sections B and C are less affected by rotation, as the locations are closer to the pole of rotation. The predicted displacement of cross sections B and C is between 12 and 15 km.

Many kinematic models of salient evolution require vertical-axis rotation and numerous studies in the region of the Helena Salient address possible vertical-axis rotations (Sussman et al., 2004, Yonkee and Weil, 2010). Along the northern border, a counter clockwise rotation of 5-14 degrees of the Campanian Two Medicine formation provides evidence to support a rotational kinematic model (Jolly and Sheriff, 1992). Along the southern border, Harlan et al. (2008) shows no vertical-axis rotation, while Eldredge and Van der Voo (1988) describe clockwise rotation of the southern portion of the salient. A finite displacement model may not be able to disprove either of these rotational histories; however it does show that rotation is possible. Rotation is a possible explanation of the greater total amount of shortening in section A on the northern portion of the salient based on the differential shortening estimates.

The results of this study complicate the applicability of previous published rotation studies within the Helena Salient that suggest counterclockwise rotation on the northern portion of the salient or a regional clockwise rotation. Counterclockwise rotation proposed by Jolly and Sheriff (1992) on the northern portion of the salient is not consistent with the eastward motion along the northern border of the salient in the models of this study. The sense of motion along the Lewis and Clark line is left lateral, which suggests thrusts beneath the line should be moving in the opposite direction of a counterclockwise rotation. However, if they are simply local block rotations, counterclockwise movement is possible because they would be rotating blocks in a regionally sinistral shear zone. Locally rotating blocks complicate the Sears (2006) theory; 5-15 of degrees regional clockwise rotation of during emplacement of the Helena Salient, with a rotational pole near Helena, Montana. To reconcile these complicating factors and the results of this study, there may be a combination of locally rotating blocks causing counterclockwise rotation along the LCL as well as regional clockwise rotation with a pole near the SWMTZ which produce the large amount of shortening in cross section A.

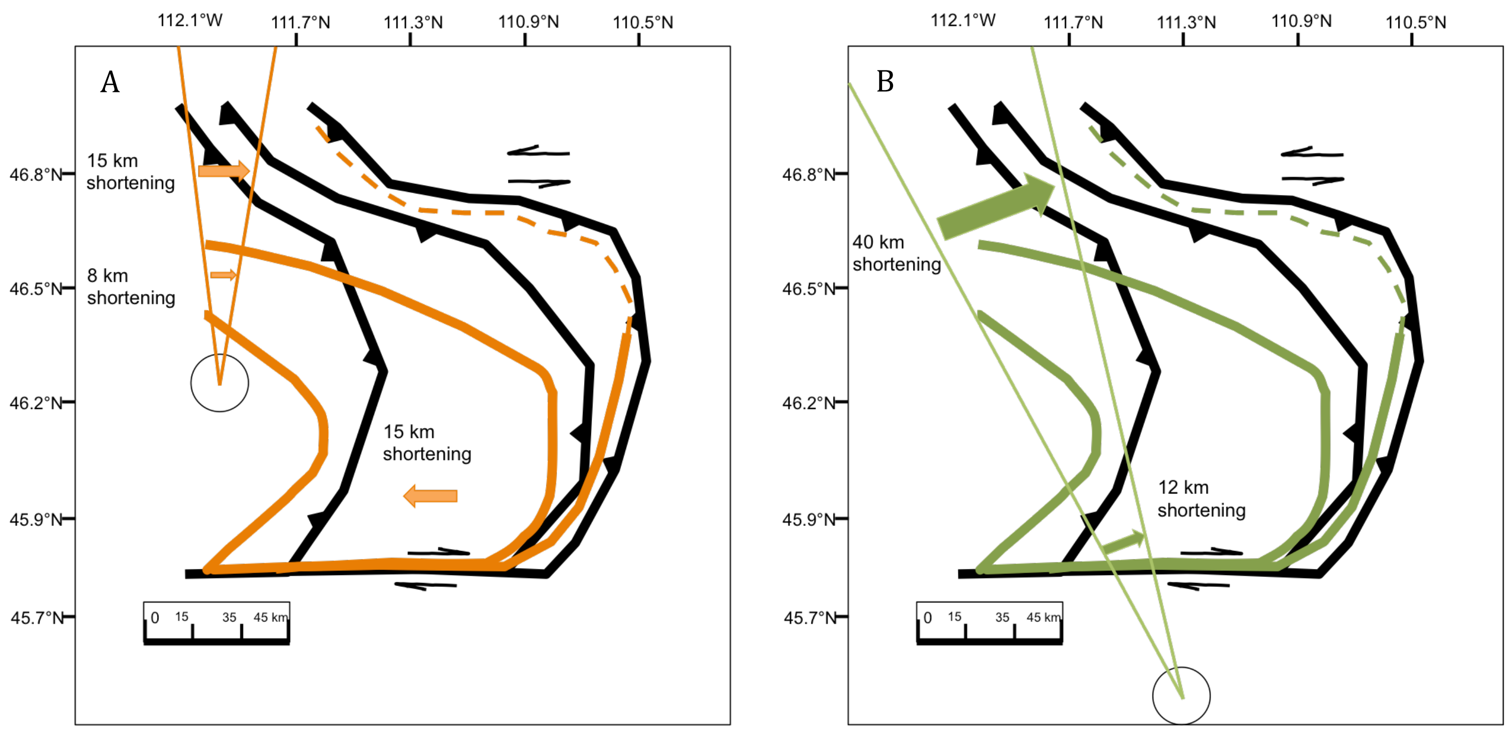

Figure 19: Possible pole locations and associated rotation which may cause differential along-strike shortening within the Helena Salient. Diagram A represents a proposed pole location from Sears (2006) which shows that this rotation cannot be used to explain shortening in the Helena Salient. Diagram B represents a pole location that can be used to describe differential along-strike shortening within the Helena Salient.

6. Conclusions

The work done in this study contributes to understanding the evolution of the Helena salient. In this study, three forward models placed in the north, central, and southern sections of the Helena Salient were used to interpret the evolution of the Helena Salient. A finite displacement model and a rotation model derived from the forward models aided interpretation. The results of this study show that the southern portion of the salient underwent uniform shortening (12-14.5 km), whereas the northern portion of the salient underwent a much greater magnitude of shortening (25 km).

Differential shortening across the Helena Salient complicates the applicability of the Macedo and Marshak (1999) basin-controlled model to the formation of the Helena Salient. Therefore, the southern portion of the salient may be described with the basin-controlled model of salient formation (Macedo and Marshak, 1999) (Figure 9). The kinematic evolution of the southern portion of the salient can be described with the primary-arc uniform translation model of Yonkee and Weil (2010) because it appears the thrusts have been uniformly translated to the east (Figure 8).

The northern portion of the salient deviates from both the basin-controlled model and the primary-arc uniform translation model. A possible cause of increased shortening in the northern portion of the salient may be rotation as Figure 19 displays the effects of a clockwise rotation from two different poles. Therefore, the evolution of the Helena Salient involves changes in salient dynamics from north to south that have strongly affected its kinematic evolution.

7. Appendix

7.1 Strike and Dip Data

X(East)	Y(North)	dip	azimuth	strike	Horizon
Metres	Metres	Degrees	Degrees	Degrees	
xy	xy	orientation	orientation	orientation	
451030.5	5190743	25	179	89	Belt
449258.2	5189626.4	8	148	58	Belt
449913.3	5189545.5	5	180	90	Belt
449893.7	5189412.3	0	90	360	Belt
450158.1	5188677.9	30	1	271	Belt
449666.1	5188333.9	30	24	294	Belt
449417.9	5188042.2	45	214	124	Belt
448917.2	5187672.1	37	20	290	Belt
448390.4	5187345.6	18	353	263	Belt
448725.6	5187397.8	38	5	275	Belt
448925.9	5187480.6	37	19	289	Belt
451427.1	5191166.8	27	181	91	Big Snowy-Kootenai
449819.8	5190952	34	92	2	Big Snowy-Kootenai
449383.1	5190987.8	20	118	28	Big Snowy-Kootenai
449476.1	5190629.8	15	126	36	Big Snowy-Kootenai
448115.8	5191177.6	36	225	135	Big Snowy-Kootenai
447911.7	5191045.1	35	233	143	Big Snowy-Kootenai
448606.2	5190261.1	70	191	101	Big Snowy-Kootenai
448448.7	5189896	51	153	63	Big Snowy-Kootenai
448713.6	5189785	50	161	71	Big Snowy-Kootenai
448087.2	5190024.9	25	190	100	Big Snowy-Kootenai
447199.4	5190096.5	50	243	153	Big Snowy-Kootenai
447016.8	5190565.4	50	179	89	Big Snowy-Kootenai
446286.5	5190583.3	35	234	144	Big Snowy-Kootenai
446633.7	5191220.5	23	174	84	Big Snowy-Kootenai
446309.7	5190074.6	40	212	122	Big Snowy-Kootenai
446320.7	5189799.3	65	120	30	Big Snowy-Kootenai
446107.8	5189241.4	51	326	236	Lodgepole- Mission Canyon
445828.8	5189142.3	85	239	149	Lodgepole- Mission Canyon
445557.2	5190254.4	33	270	180	Lodgepole- Mission Canyon
445047.1	5190353.5	67	259	169	Maywood-Threeforks
445289.3	5190052.5	25	259	169	Maywood-Threeforks
444393.7	5190177.3	45	178	88	Flathead-Maywood
445197.5	5189795.6	42	229	139	Belt

X(East)	Y(North)	dip	azimuth	strike	Horizon
Metres	Metres	Degrees	Degrees	Degrees	
xy	xy	orientation	orientation	orientation	
443714.7	5190493	32	221	131	Maywood-Threeforks
444834.2	5189700.2	24	219	129	Flathead-Maywood
443934.9	5189784.6	56	201	111	Flathead-Maywood
443769.8	5189630.4	37	208	118	Flathead-Maywood
443351.3	5190430.6	14	263	173	Flathead-Maywood
443153.1	5191271.1	23	335	245	Belt
442927.8	5190754.3	18	349	259	Belt
443058.5	5189661.1	83	44	314	Lodgepole- Mission Canyon
443461	5189066.3	85	220	130	Lodgepole- Mission Canyon
443791.9	5188847.2	80	225	135	Lodgepole- Mission Canyon
443791.9	5188453.6	32	33	303	Lodgepole- Mission Canyon
444091.6	5188176.3	45	43	313	Lodgepole- Mission Canyon
444368.9	5188757.7	38	222	132	Belt
444936.8	5188865	40	231	141	Belt
445044.2	5189039.5	53	206	116	Flathead-Maywood
443881.4	5187670.9	80	41	311	Lodgepole- Mission Canyon
444605.9	5187863.2	65	33	303	Lodgepole- Mission Canyon
444968.1	5187617.3	75	30	300	Lodgepole- Mission Canyon
445062.1	5187156.6	50	39	309	Lodgepole- Mission Canyon
443371.5	5187988.5	57	271	181	Lodgepole- Mission Canyon
442919.8	5187934.8	75	244	154	Maywood-Threeforks
443452	5186807.8	24	324	234	Maywood-Threeforks
443581.7	5187098.5	40	0	270	Maywood-Threeforks
443528.1	5187290.8	40	5	275	Maywood-Threeforks
443651.6	5186634.9	17	301	211	Flathead-Maywood
443946.2	5186205.4	28	175	85	Maywood-Threeforks
444034.8	5186040.1	20	183	93	Maywood-Threeforks
444525	5185957.4	32	206	116	Maywood-Threeforks
442877.3	5185420	45	206	116	Maywood-Threeforks
444532.1	5185548.8	20	206	116	Lodgepole- Mission Canyon
444783	5185562.7	20	218	128	Lodgepole- Mission Canyon
444469.4	5185193.5	40	222	132	Lodgepole- Mission Canyon
444497.3	5185325.8	12	192	102	Lodgepole- Mission Canyon
445040.8	5185729.9	50	215	125	Lodgepole- Mission Canyon
445674.8	5185764.8	20	42	312	Lodgepole- Mission Canyon
446274	5186468.5	75	40	310	Lodgepole- Mission Canyon
447082.2	5186029.5	80	40	310	Lodgepole- Mission Canyon
446768.7	5185778.7	70	223	133	Lodgepole- Mission Canyon

X(East)	Y(North)	dip	azimuth	strike	Horizon
Metres	Metres	Degrees	Degrees	Degrees	
xy	xy	orientation	orientation	orientation	
447312.1	5184691.8	10	68	338	Lodgepole- Mission Canyon
442908.7	5185068	35	206	116	Flathead-Maywood
443452.2	5184991.4	15	206	116	Flathead-Maywood
443863.3	5184914.8	35	204	114	Flathead-Maywood
444121.1	5185005.3	40	202	112	Flathead-Maywood
444789.9	5184552.5	80	241	151	Flathead-Maywood
445019.9	5184204.1	28	266	176	Flathead-Maywood
444824.8	5183974.2	25	263	173	Flathead-Maywood
445521.5	5182859.4	20	266	176	Flathead-Maywood
446148.6	5183166	23	246	156	Flathead-Maywood
446706	5184148.4	5	309	219	Flathead-Maywood
446880.1	5184343.4	20	316	226	Flathead-Maywood
444093.2	5184761.5	37	325	235	Belt
443793.6	5184566.4	37	261	171	Belt
443152.6	5184259.8	30	209	119	Belt
444560	5183423.7	77	199	109	Belt
444434.6	5183235.6	70	179	89	Belt
444427.6	5183242.6	25	217	127	Belt
444190.7	5182664.3	47	204	114	Belt
444274.4	5182497.1	85	204	114	Belt
444155.9	5182037.2	30	242	152	Belt
443570.6	5182051.2	38	205	115	Belt
443417.4	5181681.9	36	258	168	Belt
443089.9	5181577.4	31	266	176	Belt
443292	5181347.5	37	257	167	Belt
442922.7	5180908.5	18	255	165	Belt
443264.1	5180170	30	247	157	Belt
443898.1	5180448.7	35	231	141	Belt
444274.4	5179633.5	43	226	136	Belt
443319.8	5178734.7	45	229	139	Belt
443647.3	5177954.4	45	240	150	Belt
444351	5178100.7	42	227	137	Belt
444685.4	5178553.6	48	236	146	Belt
445640	5179306	45	201	111	Belt
445835	5179361.8	40	226	136	Belt
446155.5	5179661.4	43	226	136	Belt
446469.1	5179856.5	20	242	152	Belt
446462.1	5180051.5	34	349	259	Belt

X(East)	Y(North)	dip	azimuth	strike	Horizon
Metres	Metres	Degrees	Degrees	Degrees	
xy	xy	orientation	orientation	orientation	
449186.3	5180002.8	20	302	212	Belt
449667.1	5179793.7	25	237	147	Belt
449402.3	5178456	25	222	132	Belt
449911	5178936.8	24	225	135	Belt
451046.6	5178051.9	27	235	145	Belt
451402	5178957.7	38	208	118	Belt
450545	5179988.8	40	172	82	Lodgepole- Mission Canyon
450531.1	5179689.2	70	185	95	Lodgepole- Mission Canyon
450621.6	5180504.4	30	239	149	Lodgepole- Mission Canyon
450545	5180817.9	15	263	173	Lodgepole- Mission Canyon
448545.4	5180574.1	23	199	109	Belt
448865.9	5180622.9	50	221	131	Lodgepole- Mission Canyon
447988	5181911.8	21	268	178	Lodgepole- Mission Canyon
447813.8	5182580.7	60	197	107	Lodgepole- Mission Canyon
449311.8	5182594.6	20	207	117	Lodgepole- Mission Canyon
452043	5182887.3	80	10	280	Lodgepole- Mission Canyon
451227.8	5182692.2	30	234	144	Lodgepole- Mission Canyon
450085.1	5182531.9	35	205	115	Lodgepole- Mission Canyon
450308.1	5181842.2	10	184	94	Maywood-Threeforks
451004.8	5182086	30	248	158	Maywood-Threeforks
448948.5	5183637.3	25	47	317	Lodgepole- Mission Canyon
448628.5	5183336.7	14	58	328	Lodgepole- Mission Canyon
448114.5	5183453.1	15	27	297	Lodgepole- Mission Canyon
447842.9	5183637.3	23	93	3	Lodgepole- Mission Canyon
446378.5	5182648.1	50	239	149	Lodgepole- Mission Canyon
447018.6	5183210.6	40	239	149	Lodgepole- Mission Canyon
447416.2	5183511.3	35	273	183	Lodgepole- Mission Canyon
452061.6	5183996.2	85	199	109	Belt
449792.2	5183918.6	50	193	103	Flathead-Maywood
449491.6	5184616.8	80	23	293	Belt
449142.5	5184529.5	32	70	340	Lodgepole- Mission Canyon
446068.2	5184306.5	53	252	162	Lodgepole- Mission Canyon
446174.9	5184626.5	50	265	175	Lodgepole- Mission Canyon
451831.3	5185149.6	34	201	111	Maywood-Threeforks
450575.9	5185213.4	55	178	88	Maywood-Threeforks
449703.4	5185724.1	30	222	132	Maywood-Threeforks
450416.3	5184894.2	70	174	84	Flathead-Maywood
450288.6	5184766.5	50	174	84	Flathead-Maywood

X(East)	Y(North)	dip	azimuth	strike	Horizon
Metres	Metres	Degrees	Degrees	Degrees	
xy	xy	orientation	orientation	orientation	
447809.6	5186415.7	30	183	93	Belt
447107.4	5186447.6	10	174	84	Belt
447415.9	5186766.8	42	146	56	Flathead-Maywood
447192.5	5187181.7	8	145	55	Flathead-Maywood
446756.3	5187256.2	60	246	156	Flathead-Maywood
446479.6	5187309.4	12	20	290	Flathead-Maywood
451352.6	5185692.2	35	192	102	Lodgepole- Mission Canyon
445519.8	5188338.3	60	256	166	Flathead-Maywood
445685.5	5188212.5	85	180	90	Flathead-Maywood
445839.9	5188161.1	42	302	212	Flathead-Maywood
446011.3	5187698.1	30	78	348	Flathead-Maywood
446445.7	5187881	85	307	217	Flathead-Maywood
446948.7	5188515.4	25	198	108	Flathead-Maywood
446965.8	5188778.4	85	144	54	Flathead-Maywood
447954.6	5188098.2	66	154	64	Flathead-Maywood
448229	5188212.5	21	161	71	Flathead-Maywood
467477.7	5148064.5	80	268	178	Belt
470786.6	5145042.2	80	257	167	Belt
469692.3	5147725.8	75	92	2	Belt
471594.3	5148950.4	65	174	84	Belt
473783	5149419.4	50	31	301	Belt
473574.5	5146970.2	60	61	331	Belt
474486.4	5147986.4	20	203	113	Belt
477404.6	5149471.5	10	38	308	Belt
476753.2	5147621.6	15	53	323	Belt
480479.1	5148820.1	55	103	13	Belt
482938	5149448.7	23	29	299	Belt
483082.5	5147642.6	55	343	253	Belt
479325.9	5146270	10	34	304	Belt
475641.6	5142441.2	35	121	31	Belt
475388.7	5140707.4	25	121	31	Belt
473907.8	5139768.2	60	221	131	Belt
476291.8	5138576.2	55	221	131	Belt
496953	5147714.9	46	92	2	Belt
491715.4	5149123.6	36	78	348	Belt
494585.7	5147475.8	16	71	341	Belt
491252.6	5144368.8	45	71	341	Belt
490518.3	5141657.2	48	98	8	Belt

X(East)	Y(North)	dip	azimuth	strike	Horizon
Metres	Metres	Degrees	Degrees	Degrees	
xy	xy	orientation	orientation	orientation	
497975.2	5143973.3	51	94	4	Belt
497636.2	5142674	37	122	32	Belt
497353.8	5140131.9	37	127	37	Belt
496223.9	5138719.6	25	108	18	Belt
488823.5	5147758.3	39	68	338	Belt
488089.1	5141600.7	41	162	72	Belt
483117.8	5138437.1	43	103	13	Belt
487806.6	5134595.7	23	153	63	Belt
483400.3	5133352.9	20	117	27	Belt
480971.1	5132844.4	51	246	156	Belt
491761.1	5133465.8	35	131	41	Belt
483965.2	5131488.6	61	97	7	Belt
481310.1	5131319.2	60	253	163	Belt
477864.1	5127647.2	60	218	128	Belt
483061.3	5127534.2	25	204	114	Belt
491987	5126234.9	53	74	344	Belt
493907.8	5121941.5	35	140	50	Belt
489218.9	5118778	46	140	50	Belt
489162.6	5114578.1	41	156	66	Belt
487645.6	5114853.9	30	198	108	Belt
486404.4	5115773.3	30	240	150	Belt
483002.6	5119496.9	40	215	125	Belt
481117.9	5120600.1	51	198	108	Belt
480014.6	5122071.2	45	246	156	Belt
487461.7	5117750	35	240	150	Belt
485347.1	5120600.1	35	209	119	Belt
484059.9	5122852.7	46	209	119	Belt
480336.4	5128644.8	50	234	144	Belt
487323.8	5125518.9	35	250	160	Belt
489438.4	5131540.9	36	142	52	Belt
488105.3	5129702.1	29	126	36	Belt
497483.1	5129794.1	81	86	356	Belt
495874.1	5125243.1	88	117	27	Belt
497529	5123174.4	28	119	29	Belt
493437.7	5129702.1	27	107	17	Belt
490863.4	5122117.1	60	135	45	Belt
495938	5120711.1	20	164	74	Flathead-Maywood
494554.4	5119235.2	40	150	60	Flathead-Maywood

X(East)	Y(North)	dip	azimuth	strike	Horizon
Metres	Metres	Degrees	Degrees	Degrees	
xy	xy	orientation	orientation	orientation	
484500	5117390.4	35	218	128	Flathead-Maywood
481963.4	5119327.5	45	183	93	Flathead-Maywood
496629.8	5119419.7	10	188	98	Maywood-Threeforks
494093.2	5117390.4	39	111	21	Maywood-Threeforks
481041	5117851.6	40	219	129	Maywood-Threeforks
499489.3	5112962.8	16	252	162	Lodgepole- Mission Canyon
498705.3	5116052.9	16	207	117	Lodgepole- Mission Canyon
495338.4	5117574.9	20	129	39	Lodgepole- Mission Canyon
491648.8	5113746.8	41	137	47	Lodgepole- Mission Canyon
490126.8	5112547.7	41	166	76	Lodgepole- Mission Canyon
487221.2	5112824.4	41	202	112	Lodgepole- Mission Canyon
486298.7	5113377.9	45	207	117	Lodgepole- Mission Canyon
484915.1	5114623.1	30	246	156	Lodgepole- Mission Canyon
484822.9	5115637.8	36	246	156	Lodgepole- Mission Canyon
483116.4	5114946	31	246	156	Lodgepole- Mission Canyon
483531.5	5112178.7	31	241	151	Lodgepole- Mission Canyon
484131.1	5111025.7	46	216	126	Lodgepole- Mission Canyon
484269.4	5111902	66	222	132	Lodgepole- Mission Canyon
481363.8	5115130.4	35	236	146	Lodgepole- Mission Canyon
480441.4	5117667.1	51	236	146	Lodgepole- Mission Canyon
479242.3	5119742.5	35	241	151	Lodgepole- Mission Canyon
499627.7	5110380	25	197	107	Big Snowy-Kootenai
498843.6	5112224.8	15	235	145	Big Snowy-Kootenai
497644.5	5113516.2	25	248	158	Big Snowy-Kootenai
495430.7	5114853.7	20	248	158	Big Snowy-Kootenai
494600.5	5114715.4	35	164	74	Big Snowy-Kootenai
493493.6	5114807.6	35	158	68	Big Snowy-Kootenai
491787.1	5112732.2	61	150	60	Big Snowy-Kootenai
485560.8	5112409.3	55	249	159	Big Snowy-Kootenai
485699.2	5109227	55	90	360	Big Snowy-Kootenai
485883.7	5107566.6	40	174	84	Big Snowy-Kootenai
484961.2	5107243.8	34	263	173	Big Snowy-Kootenai
484776.8	5109134.7	70	243	153	Big Snowy-Kootenai
482747.4	5112547.7	45	253	163	Big Snowy-Kootenai
457583.2	5127486	45	294	204	Belt
456977.2	5123570.3	51	297	207	Belt
457117	5118442.5	40	239	149	Belt
457210.2	5130189.7	54	321	231	Belt

X(East)	Y(North)	dip	azimuth	strike	Horizon
Metres	Metres	Degrees	Degrees	Degrees	
xy	xy	orientation	orientation	orientation	
453061.4	5129304	35	283	193	Lodgepole- Mission Canyon
453434.3	5120447	84	247	157	Lodgepole- Mission Canyon
452548.6	5128651.4	32	283	193	Big Snowy-Kootenai
436774.4	5103305.2	19	260	170	Belt
435803.7	5105918.6	22	270	180	Belt
438006.4	5111556.1	41	106	16	Belt
438902.5	5114654.8	29	87	357	Belt
438230.4	5114206.8	33	295	205	Belt
436214.4	5111444.1	42	318	228	Belt
435617	5108233.3	30	236	146	Belt
434683.7	5103939.9	42	232	142	Flathead-Maywood
434497	5110174.7	30	297	207	Flathead-Maywood
438566.5	5116708.2	46	338	248	Flathead-Maywood
439947.8	5118425.6	19	4	274	Flathead-Maywood
440395.8	5118201.6	16	25	295	Flathead-Maywood
440769.2	5115550.8	45	103	13	Flathead-Maywood
439275.8	5102446.5	28	118	28	Flathead-Maywood
441291.9	5112825.4	15	76	346	Flathead-Maywood
436805.8	5115311.1	51	301	211	Maywood-Threeforks
438387.5	5117991.2	14	279	189	Maywood-Threeforks
439485.8	5119880.4	25	328	238	Maywood-Threeforks
440979.6	5119836.4	22	51	321	Maywood-Threeforks
442473.4	5118650.2	30	99	9	Maywood-Threeforks
442781	5109511.6	42	105	15	Maywood-Threeforks
432104.7	5108808.7	16	315	225	Lodgepole- Mission Canyon
432500.1	5115135.4	46	315	225	Lodgepole- Mission Canyon
437728.4	5119221.3	25	248	158	Lodgepole- Mission Canyon
438870.7	5121945.3	12	288	198	Lodgepole- Mission Canyon
439529.8	5122340.8	16	336	246	Lodgepole- Mission Canyon
439485.8	5125328.4	50	276	186	Lodgepole- Mission Canyon
441023.6	5121330.2	20	35	305	Lodgepole- Mission Canyon
442473.4	5119660.7	25	67	337	Lodgepole- Mission Canyon
443571.8	5112103.8	44	100	10	Lodgepole- Mission Canyon
433730.3	5120187.9	25	94	4	Big Snowy-Kootenai
434652.9	5118430.5	7	7	277	Big Snowy-Kootenai
436410.4	5119660.7	14	263	173	Big Snowy-Kootenai
437684.5	5122955.9	68	287	197	Big Snowy-Kootenai
438431.4	5125548	25	294	204	Big Snowy-Kootenai

X(East)	Y(North)	dip	azimuth	strike	Horizon
Metres	Metres	Degrees	Degrees	Degrees	
xy	xy	orientation	orientation	orientation	
494412	5096136.6	15	353	263	Belt
492600.2	5096415.3	30	16	286	Flathead-Maywood
492042.7	5097495.5	35	351	261	Maywood-Threeforks
496432.8	5097251.6	40	74	344	Maywood-Threeforks
492356.3	5098749.8	20	307	217	Lodgepole- Mission Canyon
492495.6	5099551.2	80	348	258	Big Snowy-Kootenai
477009.9	5109954.9	20	337	247	Belt
476514.5	5109040.3	25	262	172	Belt
477848.3	5109573.8	30	47	317	Belt
479296.5	5107630.3	41	10	280	Belt
477886.4	5105420	15	337	247	Belt
479334.6	5102561.8	66	311	221	Belt
477314.8	5098979.5	66	109	19	Belt
476476.4	5096769.2	70	139	49	Belt
478953.5	5100008.5	80	111	21	Flathead-Maywood
480096.7	5104162.4	40	95	5	Flathead-Maywood
479982.4	5100732.6	10	81	351	Maywood-Threeforks
478458.1	5095930.8	25	333	243	Maywood-Threeforks
480173	5098903.3	25	63	333	Lodgepole- Mission Canyon
482078.4	5102447.5	35	239	149	Lodgepole- Mission Canyon
461309	5099246.3	85	291	201	Belt
465158	5103857.5	40	309	219	Belt
469883.5	5113613.4	30	303	213	Belt
468168.6	5109726.3	20	323	233	Belt
463559.1	5099410.9	45	323	233	Flathead-Maywood
464341.4	5099247.9	40	301	211	Maywood-Threeforks
462320.4	5096086	65	301	211	Maywood-Threeforks
466036.5	5103224.7	25	347	257	Maywood-Threeforks
471761.2	5112287.1	21	344	254	Maywood-Threeforks
470617.4	5110293.8	15	304	214	Maywood-Threeforks
465389.1	5100392.6	70	107	17	Lodgepole- Mission Canyon
473035.6	5110457.2	20	288	198	Lodgepole- Mission Canyon
473591.1	5111568.2	8	297	207	Lodgepole- Mission Canyon
470748.2	5106535.9	15	288	198	Lodgepole- Mission Canyon
498655.4	5084688.9	20	9	279	Belt
485041	5086762.2	10	337	247	Belt
483555.1	5083686.9	16	328	238	Belt
477024.3	5083894.2	25	15	285	Belt

X(East)	Y(North)	dip	azimuth	strike	Horizon
Metres	Metres	Degrees	Degrees	Degrees	
xy	xy	orientation	orientation	orientation	
472117.6	5087004.1	75	327	237	Maywood-Threeforks
485732.1	5090044.9	22	343	253	Maywood-Threeforks
476678.8	5094260.5	36	309	219	Maywood-Threeforks
470873.6	5091738.1	41	301	211	Maywood-Threeforks
468973.1	5091081.5	24	293	203	Maywood-Threeforks
468420.3	5091530.7	18	129	39	Maywood-Threeforks
465344.9	5092601.9	51	301	211	Maywood-Threeforks
461647.6	5094295.1	60	164	74	Maywood-Threeforks
461198.4	5094398.8	15	261	171	Maywood-Threeforks
466174.2	5088178.9	25	312	222	Maywood-Threeforks
467936.5	5089353.8	20	305	215	Maywood-Threeforks
496202.1	5092256.4	40	17	287	Belt
497998.9	5092221.8	70	223	133	Lodgepole- Mission Canyon
497549.7	5094640.6	65	279	189	Big Snowy-Kootenai
474363.6	5087798.9	40	141	51	Lodgepole- Mission Canyon
468143.8	5084101.5	64	317	227	Lodgepole- Mission Canyon
471633.8	5089042.8	48	338	248	Lodgepole- Mission Canyon
466347	5087868	80	329	239	Lodgepole- Mission Canyon
466036	5089077.4	29	325	235	Lodgepole- Mission Canyon
464653.8	5089111.9	25	108	18	Lodgepole- Mission Canyon
465759.6	5094226	40	302	212	Lodgepole- Mission Canyon
482864	5091427.1	23	319	229	Big Snowy-Kootenai
478406.5	5088144.4	25	346	256	Big Snowy-Kootenai
467591	5084999.9	17	22	292	Big Snowy-Kootenai
469906.1	5087038.7	28	145	55	Big Snowy-Kootenai
502965.2	5065059.2	48	296	206	Lodgepole- Mission Canyon
511909.3	5107578.1	48	252	162	Big Snowy-Kootenai
510302.6	5105275.1	25	240	150	Big Snowy-Kootenai
512284.2	5113898	25	86	356	Big Snowy-Kootenai
501733.3	5103186.3	15	256	166	Big Snowy-Kootenai
502215.3	5104900.2	25	222	132	Lodgepole- Mission Canyon
502268.8	5106346.2	41	300	210	Lodgepole- Mission Canyon
502108.2	5110684.5	20	203	113	Lodgepole- Mission Canyon
506499.9	5113844.4	50	128	38	Lodgepole- Mission Canyon
501358.3	5115129.8	15	214	124	Maywood-Threeforks
503377.1	5111844.6	15	232	142	Maywood-Threeforks
511875.2	5132419.1	50	167	77	Maywood-Threeforks
513564.9	5132220.3	70	225	135	Maywood-Threeforks

X(East)	Y(North)	dip	azimuth	strike	Horizon
Metres	Metres	Degrees	Degrees	Degrees	
xy	xy	orientation	orientation	orientation	
513415.8	5131623.9	56	252	162	Lodgepole- Mission Canyon
514558.9	5128741.5	66	86	356	Lodgepole- Mission Canyon
514012.2	5126902.7	30	117	27	Lodgepole- Mission Canyon
513714	5126604.5	55	233	143	Lodgepole- Mission Canyon
501389.3	5141513.5	12	150	60	Belt
502333.5	5140171.7	16	127	37	Belt
501637.7	5136543.9	16	127	37	Belt
504718.9	5134804.5	20	164	74	Belt
501985.6	5132965.7	10	164	74	Belt
506259.5	5134854.2	65	84	354	Belt
510682.5	5146234.7	40	214	124	Maywood-Threeforks
510434	5146831.1	20	225	135	Flathead-Maywood
513962.5	5144147.5	59	225	135	Flathead-Maywood
513167.4	5148868.6	47	236	146	Belt
512322.5	5147974.1	38	236	146	Belt
520572.2	5141612.9	21	236	146	Belt
512620.7	5141811.7	10	81	351	Big Snowy-Kootenai
512670.4	5143948.7	50	217	127	Lodgepole- Mission Canyon
509887.4	5145539	35	233	143	Lodgepole- Mission Canyon
512123.7	5142805.6	60	195	105	Maywood-Threeforks
512372.2	5140619	50	87	357	Maywood-Threeforks
510732.2	5142457.8	18	29	299	Lodgepole- Mission Canyon
510632.8	5141911.1	38	225	135	Lodgepole- Mission Canyon
531300.8	5146177.9	25	94	4	Big Snowy-Kootenai
531331.7	5149573.8	51	186	96	Big Snowy-Kootenai
540654.9	5146980.6	46	194	104	Big Snowy-Kootenai
544946.1	5142380.7	23	170	80	Big Snowy-Kootenai
545254.8	5147073.2	25	252	162	Big Snowy-Kootenai
543680.3	5143214.2	45	231	141	Big Snowy-Kootenai
535715.5	5148215.4	12	122	32	Big Snowy-Kootenai
534696.7	5146702.7	20	210	120	Big Snowy-Kootenai
540130.1	5147937.6	45	196	106	Lodgepole- Mission Canyon
538617.4	5149079.8	50	225	135	Lodgepole- Mission Canyon
540408	5148832.9	58	207	117	Maywood-Threeforks
542445.5	5148184.6	21	218	128	Flathead-Maywood
541210.6	5149234.2	20	198	108	Flathead-Maywood
542105.9	5148153.7	68	168	78	Flathead-Maywood
534573.2	5148400.7	5	253	163	Big Snowy-Kootenai

X(East)	Y(North)	dip	azimuth	strike	Horizon
Metres	Metres	Degrees	Degrees	Degrees	
xy	xy	orientation	orientation	orientation	
510753.8	5182128.7	17	230	140	Flathead-Maywood
503589.4	5180451.9	5	195	105	Flathead-Maywood
512989.5	5178622.7	51	275	185	Flathead-Maywood
525793.9	5187667.1	7	177	87	Flathead-Maywood
532094.5	5187311.4	10	347	257	Flathead-Maywood
528080.4	5185939.5	8	347	257	Flathead-Maywood
524625.2	5182382.7	3	166	76	Flathead-Maywood
538699.9	5179130.8	3	280	190	Flathead-Maywood
516840.8	5178458	3	191	101	Flathead-Maywood
524465	5179930.8	7	181	91	Flathead-Maywood
505837.7	5179627.6	48	341	251	Belt
504278.2	5178587.9	30	351	261	Belt
501029.3	5177158.4	40	198	108	Belt
503368.5	5174169.4	32	199	109	Belt
509130	5167714.8	18	199	109	Belt
507050.7	5165375.6	29	206	116	Belt
516624.2	5164942.4	20	206	116	Belt
517837.1	5167931.4	8	193	103	Belt
512985.4	5170833.8	25	231	141	Belt
519093.4	5172869.8	23	203	113	Belt
526457.6	5172393.3	18	203	113	Belt
530269.7	5170487.3	28	230	140	Belt
531742.6	5166242	10	252	162	Belt
536247.8	5166891.8	23	207	117	Belt
537980.5	5164509.2	35	238	148	Belt
535164.8	5164162.7	15	74	344	Belt
543178.8	5163902.7	15	159	69	Belt
546037.9	5167065	27	155	65	Belt
545864.6	5172653.2	10	142	52	Belt
541749.3	5150603.8	15	45	315	Belt
539280.1	5153506.1	30	225	135	Belt
542095.9	5152856.4	42	115	25	Belt
528710.2	5161953.4	51	202	112	Belt
531266.1	5159484.2	30	216	126	Belt
532479	5155628.8	37	247	157	Belt
535814.6	5154979	31	176	86	Belt
537763.9	5155975.3	41	238	148	Belt
539236.8	5158098	37	257	167	Belt

X(East)	Y(North)	dip	azimuth	strike	Horizon
Metres	Metres	Degrees	Degrees	Degrees	
xy	xy	orientation	orientation	orientation	
506314.2	5164076	38	225	135	Flathead-Maywood
510039.7	5161476.9	40	225	135	Flathead-Maywood
517620.5	5162213.3	60	182	92	Flathead-Maywood
521692.5	5162256.6	43	193	103	Flathead-Maywood
540131.1	5163653.7	28	216	126	Flathead-Maywood
538413.7	5151643.4	22	225	135	Flathead-Maywood
543135.5	5152293.2	45	101	11	Flathead-Maywood
545128.2	5162646.5	12	163	73	Flathead-Maywood
550933	5168884.4	18	176	86	Flathead-Maywood
555524.8	5167584.9	10	176	86	Flathead-Maywood
543143.6	5151085.9	22	107	17	Maywood-Threeforks
540131.1	5163653.7	14	106	16	Maywood-Threeforks
540648.9	5163512.5	10	236	146	Maywood-Threeforks
552416.5	5168831.4	12	184	94	Maywood-Threeforks
555946.7	5165536.5	42	6	276	Maywood-Threeforks
536742.1	5170243.5	10	254	164	Maywood-Threeforks
506757.1	5162652.2	40	212	122	Maywood-Threeforks
503279.8	5164771.1	36	200	110	Maywood-Threeforks
503062.5	5164390.8	12	35	305	Maywood-Threeforks
530174.3	5185906.4	35	22	292	Belt
528924.6	5181668.5	27	259	169	Belt
530826.3	5184602.4	10	249	159	Belt
542624.6	5159735.8	23	200	110	Lodgepole- Mission Canyon
547169.5	5161235.2	42	143	53	Lodgepole- Mission Canyon
542343.4	5160860.4	35	198	108	Lodgepole- Mission Canyon
526787.7	5159220.4	20	207	117	Lodgepole- Mission Canyon
528333.9	5158236.5	50	221	131	Lodgepole- Mission Canyon
530723.5	5153457.3	39	229	139	Lodgepole- Mission Canyon
534005.6	5170792.5	10	209	119	Lodgepole- Mission Canyon
532209.2	5175915.6	8	201	111	Lodgepole- Mission Canyon
532209.2	5178310.9	3	177	87	Lodgepole- Mission Canyon
534671	5180107.3	7	167	77	Lodgepole- Mission Canyon
526221.1	5174917.6	6	170	80	Lodgepole- Mission Canyon
526287.6	5178177.8	10	179	89	Lodgepole- Mission Canyon
524291.6	5175782.6	7	191	101	Lodgepole- Mission Canyon
518835.8	5176115.2	10	344	254	Lodgepole- Mission Canyon
538130.8	5173187.7	8	218	128	Lodgepole- Mission Canyon
528637.9	5151943.9	22	65	335	Big Snowy-Kootenai

7.2 Geologic Basemap

Geological Map References (included in References, section 8):

Berg, R.B., Lopez, D.A., Lonn, J.D., 2000, Geologic map of the Livingston 30' x 60' quadrangle, south-central Montana, Montana Bureau of Mines and Geology: Open-File Report 406, 21 p., 1 sheet, 1:100,000.

Lopez, D.A., 2000, Geologic map of the Big Timber 30' x 60' quadrangle, south-central Montana, Montana Bureau of Mines and Geology: Open-File Report 405, 1 sheet, 1:100,000.

Marshak, Stephen, and M. Scott Wilkerson. "Effect of overburden thickness on thrust belt geometry and development." *Tectonics* 11.3 (1992): 560-566.

McDonald, C., Lopez, D.A., Berg, R.B., Gibson, R.I., 2005, Preliminary geologic map of the Ringling 30' x 60' quadrangle, central Montana, Montana Bureau of Mines and Geology: Open-File Report 511, 27 p., 1 sheet, 1:100,000.

Porter, K.W., Wilde, E.M., Vuke, S.M., 1999, The preliminary geologic map of the Big Snowy Mountains 30' x 60' quadrangle, Montana, revised 1999, Montana Bureau of Mines and Geology: Open-File Report 341, 16 p., 1 sheet, 1:100,000.

Reynolds, M.W., and Brandt, T.R., 2007, Preliminary geologic map of the White Sulphur Springs 30' x 60' quadrangle, Montana: U.S. Geological Survey Open-File Report 2006-1329, scale 1:100,000.

Reynolds, M.W., and Brandt, T.R., 2006, Geologic map of the Canyon Ferry Dam 30' x 60' quadrangle, West- Central Montana: U.S. Geological Survey Open-File Report 2006-1329, scale 1:100,000.

Reynolds, M.W., and Brandt, T.R., 2006, Preliminary Geologic Map of the Townsend 30'x 60' Quadrangle, Montana: U.S. Geological Survey Open-File Report 2006, scale 1:100,000.

Vuke, S.M., Lonn, J.D., Berg, R.B., Schmidt, C.J., 2014, Geologic map of the Bozeman 30' x 60' quadrangle, southwestern Montana, Montana Bureau of Mines and Geology: Open-File Report 648, 44 p., 1 sheet, 1:100,000.

Wilde, E.M., Porter, K.W., 2001, Geologic map of the Harlowton 30' x 60' quadrangle, eastern Montana, Montana Bureau of Mines and Geology: Open-File Report 434, 20 p., 1 sheet, 1:100,000.

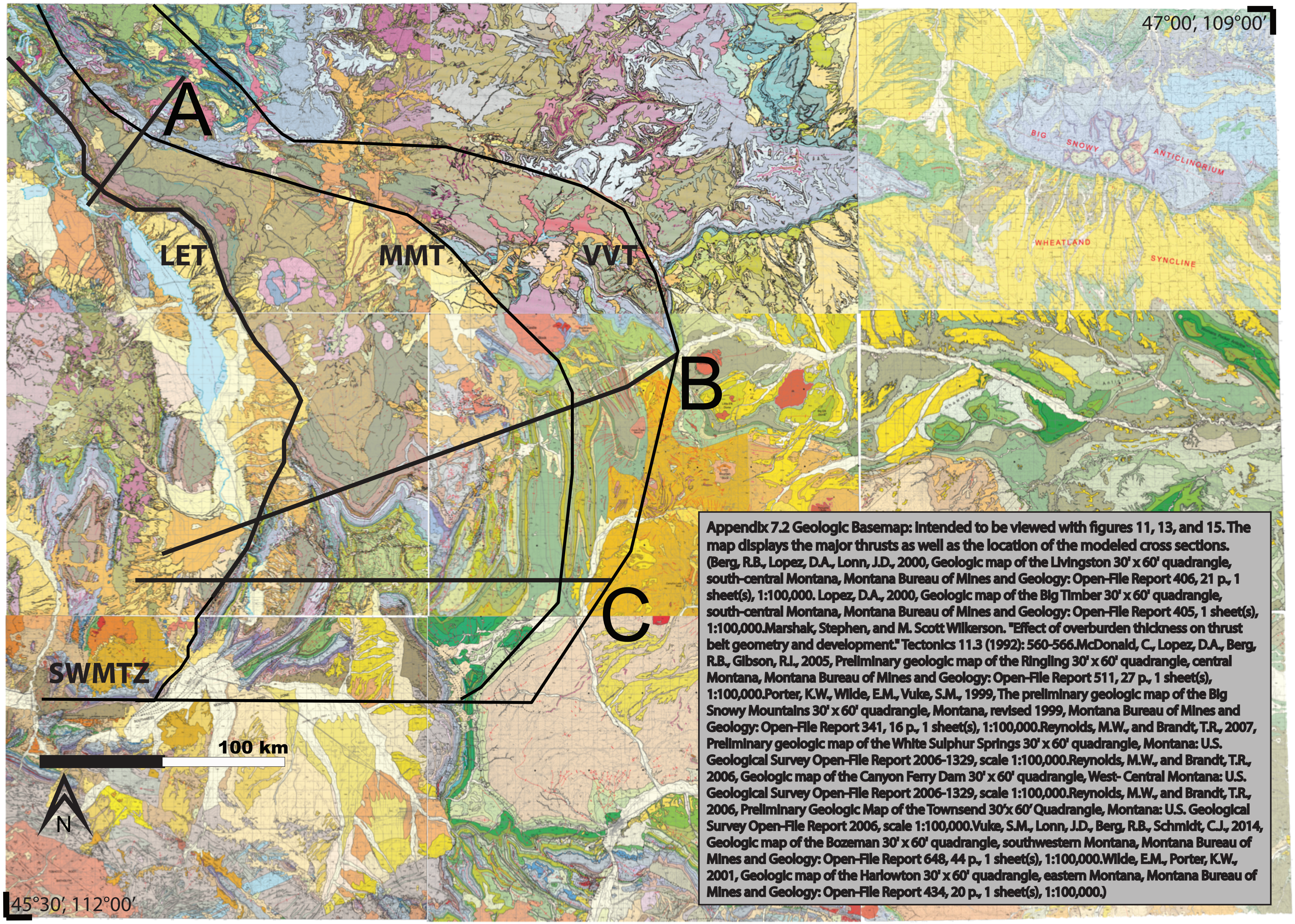

Appendix 7.2 Geologic Basemap: intended to be viewed with figures 11, 13, and 15. The map displays the major thrusts as well as the location of the modeled cross sections. (Berg, R.B., Lopez, D.A., Lonn, J.D., 2000, Geologic map of the Livingston 30' x 60' quadrangle, south-central Montana, Montana Bureau of Mines and Geology: Open-File Report 406, 21 p., 1 sheet(s), 1:100,000. Lopez, D.A., 2000, Geologic map of the Big Timber 30' x 60' quadrangle, south-central Montana, Montana Bureau of Mines and Geology: Open-File Report 405, 1 sheet(s), 1:100,000.Marshak, Stephen, and M. Scott Wilkerson. "Effect of overburden thickness on thrust belt geometry and development." Tectonics 11.3 (1992): 560-566.McDonald, C., Lopez, D.A., Berg, R.B., Gibson, R.I., 2005, Preliminary geologic map of the Ringling 30' x 60' quadrangle, central Montana, Montana Bureau of Mines and Geology: Open-File Report 511, 27 p., 1 sheet(s), 1:100,000.Porter, K.W., Wilde, E.M., Vuke, S.M., 1999, The preliminary geologic map of the Big Snowy Mountains 30' x 60' quadrangle, Montana, revised 1999, Montana Bureau of Mines and Geology: Open-File Report 341, 16 p., 1 sheet(s), 1:100,000.Reynolds, M.W., and Brandt, T.R., 2007, Preliminary geologic map of the White Sulphur Springs 30' x 60' quadrangle, Montana: U.S. Geological Survey Open-File Report 2006-1329, scale 1:100,000.Reynolds, M.W., and Brandt, T.R., 2006, Geologic map of the Canyon Ferry Dam 30' x 60' quadrangle, West- Central Montana: U.S. Geological Survey Open-File Report 2006-1329, scale 1:100,000.Reynolds, M.W., and Brandt, T.R., 2006, Preliminary Geologic Map of the Townsend 30'x 60' Quadrangle, Montana: U.S. Geological Survey Open-File Report 2006, scale 1:100,000.Vuke, S.M., Lonn, J.D., Berg, R.B., Schmidt, C.J., 2014, Geologic map of the Bozeman 30' x 60' quadrangle, southwestern Montana, Montana Bureau of Mines and Geology: Open-File Report 648, 44 p., 1 sheet(s), 1:100,000.Wilde, E.M., Porter, K.W., 2001, Geologic map of the Harlowton 30' x 60' quadrangle, eastern Montana, Montana Bureau of Mines and Geology: Open-File Report 434, 20 p., 1 sheet(s), 1:100,000.)

Map Units

Unit	Description
Qal	Alluvium of modern channels and flood plains
Qc	Colluvium
Qac	Alluvium and colluvium, undivided
Qaf	Alluvial fan deposit
Qlk	Lake deposit
Qta	Talus deposit
Qls	Landslide deposit
Qpg	Pediment gravel deposit
Qg	Glacial deposit, undivided
Qat	Alluvium of alluvial terrace
Qat1	Alluvium of youngest alluvial terrace
Qat2	Alluvium of second youngest alluvial terrace
Qat3	Alluvium of third youngest alluvial terrace
Qat4	Alluvium of fourth youngest alluvial terrace
Qat5	Alluvium of fifth youngest alluvial terrace, oldest
Qao	Alluvium, older, undivided
QTaf	Alluvial fan deposit
Ts	Sediment or sedimentary rocks, undivided
Tsuc	Sediment or sedimentary rock, upper Ter. coarser-grained
Tbh	Basalt, hypabyssal
Tai	Alkalic Intrusive
Tdio	Diorite
Tsy	Syenite
Tav	Absaroka Volcanics
Tftr	Tongue River Member of Fort Union Formation
Tfle	Lebo Member of Fort Union Formation
Tft	Tullock Member of Fort Union Formation
TKfu	Fort Union Formation, undivided
Khc	Hell Creek Formation
Kdi	Diorite
Klsr	Sliderock Mtn. Fm., informal, of Livingston Group
Kho	Hoppers Formation
Kbc	Billman Creek Formation
Kmi	Miner Creek Formation
Kcd	Cokedale Formation
Kse	Sedan Formation
Ksle	Lennep Sandstone Member, of Sedan Formation
Ksmu	Mudstone member, informal, of Sedan Formation
Ksms	Middle sandstone member, informal, of Sedan Formation
Ksa	Ash-flow tuff member, informal, of Sedan Formation
Ksls	Lower sandstone member, informal, of Sedan Formation
Kjre	Judith River through Eagle Formations, undivided
Ke	Eagle Formation
Ket	Eagle and Telegraph Creek Formations, undivided
Ktc	Telegraph Creek Formation
Kn	Niobrara Formation
Kco	Cody Shale
Kcou	Upper shale member, informal, of Cody Shale
Kce	Eldridge Creek Member of Cody Shale
Kcol	Lower shale member, informal, of Cody Shale
Kclf	Lower shale member, informal, of Cody Shale and Frontier Formation, undivided
Kcof	Cody Shale and Frontier Formation, undivided
Kf	Frontier Formation
Kmfr	Mowry through Fall River Formations, undivided
Kk	Kootenai Formation
Jme	Morrison Formation and Ellis Group, undivided
Jm	Morrison Formation
Je	Ellis Group, undivided
PMpa	Phosphoria, Quadrant, and Amsden Formations, undivided
ℙMqa	Quadrant and Amsden Formations, undivided
ℙq	Quadrant Formation
ℙMa	Amsden Formation
Msr	Snowcrest Range Group
Mm	Madison Group, undivided
Mmc	Mission Canyon Limestone
Ml	Lodgepole Limestone
MDtm	Three Forks Formation, Jefferson Dolomite and Maywood Formation
MDtm	Three Forks Formation, Jefferson Dolomite and Maywood Formation
DOs	Sedimentary rocks, undivided
OꞒsp	Snowy Range Formation and Pilgrim Limestone
Ꞓs	Sedimentary rocks, undivided
Ꞓgs	Grove Creek and Snowy Range Formations, undivided
Ꞓpi	Pilgrim Limestone
Ꞓpf	Park through Flathead Formations, undivided
Ꞓp	Park Shale
Ꞓm	Meagher Limestone
Ꞓw	Wolsey Shale
Ꞓf	Flathead Formation
Yla	Lahood Formation
Asw	Stillwater Complex
Asw7	Upper zones - Stillwater Complex
Asw6	Middle anorthosite zone - Stillwater Complex
Asw5	Lower and middle zones - Stillwater Complex
Asw4	Lower anorthosite zone - Stillwater Complex
Asw3	Norite and lower gabbro zones - Stillwater Complex
Aga	Amphibolite and gneiss
Agn	Gneissic rocks
Aqa	Quartzite and amphibolite
Aqfg	Quartzofeldspathic gneiss
As	Biotite schist
Asm	Sillimanite-garnet-biotite gneiss and marble
Anc	Nappe core complex

8. References

Bregman, M. L. "Change in tectonic style along the Montana Thrust Belt." In: *Geology* (ed.): 4.12 (1976): 775-778.

Berg, R.B., Lopez, D.A., Lonn, J.D., 2000, Geologic map of the Livingston 30' x 60' quadrangle, south-central Montana, Montana Bureau of Mines and Geology: Open-File Report 406, 21 p., 1 sheet, 1:100,000.

DeCelles, Peter G. "Late Jurassic to Eocene evolution of the Cordilleran thrust belt and foreland basin system, western USA." In: *American Journal of Science* (ed.): 304.2 (2004): 105-168.

Eldredge, Sarah, and Rob Van der Voo. "Paleomagnetic study of thrust sheet rotations in the Helena and Wyoming salients of the northern Rocky Mountains." In: *Interaction of the Rocky Mountain foreland and the Cordilleran thrust belt: Geological Society of America Memoir* (ed.): 171 (1988): 319-332.

Fryxell, Jenny C. and Donald L. Smith. "Paleotectonic implications of arkose beds in Park Shale (Middle Cambrian), Bridger Range, South-Central Montana: ABSTRACT." In: *AAPG Bulletin* (ed.): 67 (1983): 159-171.

Fuentes, Facundo, Peter G. DeCelles, and Kurt N. Constenius. "Regional structure and kinematic history of the Cordilleran fold-thrust belt in Northwest Montana, USA." In: *Geosphere* (ed.): 8.5 (2012): 1104-128.

Harlan, Stephen S., John Wm. Geissman, Stephen C. Whisner, and Christopher J. Schmidt. "Paleomagnetism and geochronology of sills of the Doherty Mountain area, Southwestern Montana: Implications for the timing of fold-and-thrust belt deformation and vertical-axis rotations along the southern margin of the Helena Salient." In: *Geological Society of America Bulletin* (ed.): 120.9 (2008): 1091-1104.

Jolly, Arthur D., and Steven D. Sheriff. "Paleomagnetic study of thrust-sheet motion along the Rocky Mountain front in Montana." In: *Geological Society of America Bulletin* (ed.): 104.6 (1992): 779-785.

Kalakay, Thomas J., Barbara E. John, and David R. Lageson. "Fault-controlled pluton emplacement in the Sevier fold-and-thrust belt of Southwest Montana, USA." In: *Journal of Structural Geology* (ed.): 23 (2001): 1151-165.

Lageson, David R., James G. Schmitt, Brian K. Horton, Thomas J. Kalakay, and Bradford R. Burton. "Influence of Late Cretaceous Magmatism on the Sevier Orogenic Wedge, Western Montana." In: *Geology* (ed.): 29.8 (2001): 723-726.

Lopez, D.A., 2000, Geologic map of the Big Timber 30' x 60' quadrangle, south-central Montana, Montana Bureau of Mines and Geology: Open-File Report 405, 1 sheet, 1:100,000.

Macedo, Juliano, and Stephen Marshak. "Controls on the geometry of fold-thrust belt salients." In: *Geological Society of America Bulletin* (ed.): 111.12 (1999): 1808-1822.

McDonald, C., Lopez, D.A., Berg, R.B., Gibson, R.I., 2005, Preliminary geologic map of the Ringling 30' x 60' quadrangle, central Montana, Montana Bureau of Mines and Geology: Open-File Report 511, 27 p., 1 sheet, 1:100,000.

McMechan, M. E., and R. I. Thompson. "The Canadian Cordilleran fold and thrust belt south of 66 N and its influence on the Western Interior Basin." In: *Evolution of the Western Interior Basin: Geological Association of Canada Special Paper* (ed.): 39 (1993): 73-90.

Peterson, J. A. "General stratigraphy and regional paleotectonics of the Western Montana Overthrust Belt." In: *Symposium Guidebook to the Southwest Montana Geological Society* (1981): 5-35.

Platt, J. P., and R. L. M. Vissers. "Extensional collapse of thickened continental lithosphere; A working hypothesis for the Alboran Sea and Gibraltar Arc." In: *Geology* (ed.): 17.6 (1989): 540-543.

Porter, K.W., Wilde, E.M., Vuke, S.M., 1999, The preliminary geologic map of the Big Snowy Mountains 30' x 60' quadrangle, Montana, revised 1999, Montana Bureau of Mines and Geology: Open-File Report 341, 16 p., 1 sheet, 1:100,000.

Price, Raymond A., and James W. Sears. "A preliminary palinspastic map of the Mesoproterozoic Belt-Purcell Supergroup, Canada and USA: Implications for the tectonic setting and structural evolution of the Purcell anticlinorium and the Sullivan deposit." In: *Mineral Deposits Division, Special Publication* (ed.): 1 (2000): 61-81.

Reynolds, M.W., and Brandt, T.R., 2007, Preliminary geologic map of the White Sulphur Springs 30' x 60' quadrangle, Montana: U.S. Geological Survey Open-File Report 2006-1329, scale 1:100,000.

Reynolds, M.W., and Brandt, T.R., 2006, Geologic map of the Canyon Ferry Dam 30' x 60' quadrangle, West- Central Montana: U.S. Geological Survey Open-File Report 2006-1329, scale 1:100,000.

Ryan, W.B.F., S.M. Carbotte, J.O. Coplan, S. O'Hara, A. Melkonian, R. Arko, R.A. Weissel, V. Ferrini, A. Goodwillie, F. Nitsche, J. Bonczkowski, and R. Zemsky (2009), Global multi-resolution topography synthesis, Geochem. Geophys. Geosyst., 10, Q03014, doi:10.1029/2008GC002332.

Sears, James W. "Montana transform: A tectonic cam surface linking thin- and thick-skinned Laramide shortening across the Rocky Mountain foreland." In: *Rocky Mountain Geology* (ed.): 41.2 (2006): 65-76.

Sears, J. W. "Belt-Purcell basin: Keystone of the Rocky Mountain fold-and-thrust belt, United States and Canada." In: *Special Paper - Geological Society Of America* (ed.): 433 (2007): 147-166.

Schmidt, Christopher J., and J. Michael O'Neill. "Structural evolution of the southwest Montana transverse zone." In: *Rocky Mountain Association of Geologists* (ed.): 1 (1982): 193-218.

Sussman, A. J., Butler, R. F., Dinarès-Turell, J., & Vergés, J. "Vertical-axis rotation of a foreland fold and implications for orogenic curvature: an example from the Southern Pyrenees, Spain." In: *Earth and Planetary Science Letters* (ed.): *218*.3 (2004): 435-449.

Tilling, Robert I. "Structural State And Perthitization Of Alkali Feldspars From An Epizonal Pluton, Boulder Batholith, Montana." In: *Special Paper - Geological Society Of America* (1968): 220-221.

Vuke, S.M., Lonn, J.D., Berg, R.B., Schmidt, C.J., 2014, Geologic map of the Bozeman 30' x 60' quadrangle, southwestern Montana, Montana Bureau of Mines and Geology: Open-File Report 648, 44 p., 1 sheet, 1:100,000.

Wallace, C. A., D. J. Lidke, and R. G. Schmidt. "Faults of the central part of the Lewis and Clark line and fragmentation of the Late Cretaceous foreland basin in west-central Montana." In: *Geological Society of America Bulletin* (ed.): 102.8 (1990): 1021-1037.

Wilde, E.M., Porter, K.W., 2001, Geologic map of the Harlowton 30' x 60' quadrangle, eastern Montana, Montana Bureau of Mines and Geology: Open-File Report 434, 20 p., 1 sheet, 1:100,000.

Winston, Don. "Middle Proterozoic Belt Basin syndepositional faults and their influence on Phanerozoic thrusting and extension." In: *AAPG Meeting Abstract* (ed.): 67.8 (1983): 1361.

Woodward, Lee A. "Tectonic framework of disturbed belt of west-central Montana." In: *AAPG Bulletin* (ed.): 65 (1981): 291-302.

Yonkee, Adolph, and Arlo B. Weil. "Reconstructing the kinematic evolution of curved mountain belts: Internal strain patterns in the Wyoming Salient, Sevier Thrust Belt, USA." In: *Geological Society of America Bulletin* (ed.): 122.1/2 (2010): 24-49.